CONF-930496--3

UCRL-JC-112444
PREPRINT

The Analysis of Repository-Heat-Driven Hydrothermal Flow at Yucca Mountain

T.A. Buscheck
J.J. Nitao

This paper was prepared for submittal to the
American Nuclear Society
International High Level Radioactive Waste Management Conference
Las Vegas, Nevada
April 26-30, 1993

January 1993

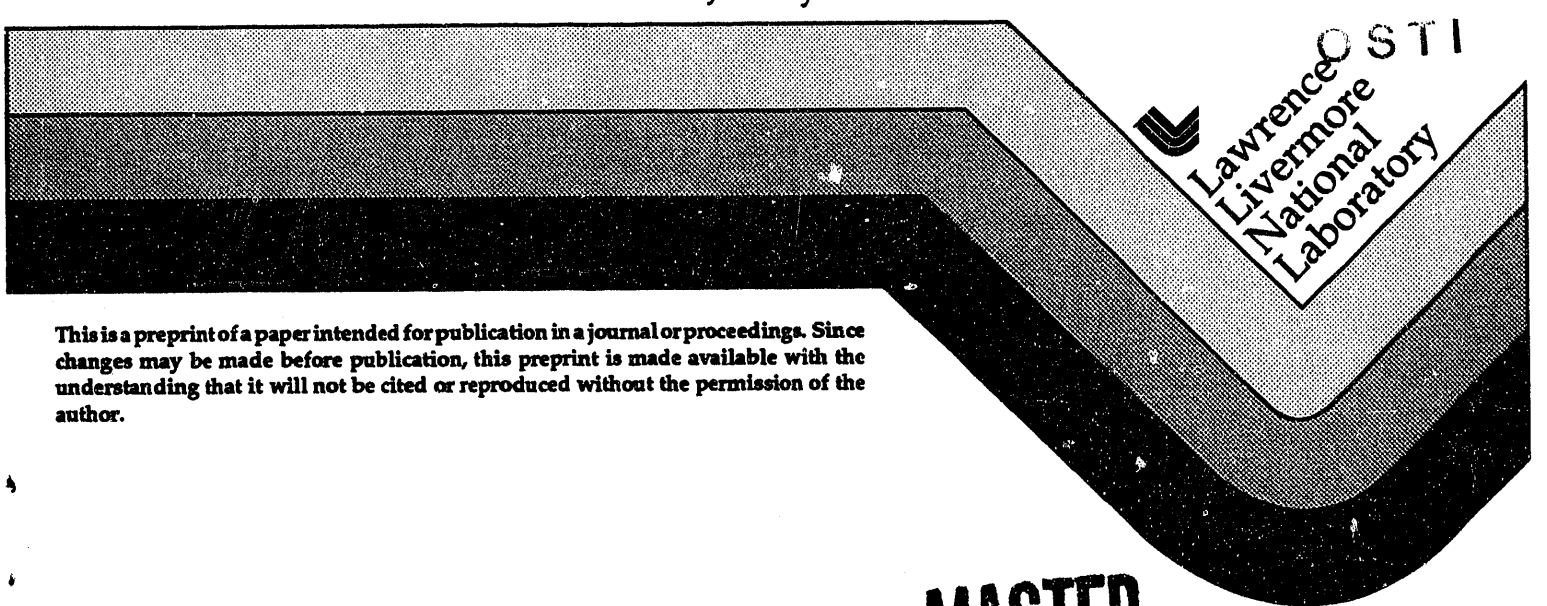

DISCLAIMER

THE ANALYSIS OF REPOSITORY-HEAT-DRIVEN HYDROTHERMAL FLOW AT YUCCA MOUNTAIN

UCRL-JC--112444

DE93 009062

Thomas A. Buscheck and John J. Nitao

Earth Sciences Department, L-206, P.O. Box 808

Lawrence Livermore National Laboratory, Livermore, CA 94551

telephone: (510) 423-9390, (510) 423-0297

ABSTRACT

To safely and permanently store high-level nuclear waste, the potential Yucca Mountain repository site must mitigate the release and transport of radionuclides for tens of thousands of years. In the failure scenario of greatest concern, water would contact the waste package (WP), accelerate its failure rate, and eventually transport radionuclides to the water table. In a concept called the "extended-dry repository," decay heat arising from radioactive waste extends the time before liquid water can contact a WP. Recent modeling and theoretical advances in nonisothermal, multiphase fracture-matrix flow have demonstrated (1) the critical importance of capillary pressure disequilibrium between fracture and matrix flow, and (2) that radioactive decay heat plays a dominant role in the ability of the engineered and natural barriers to contain and isolate radionuclides. Our analyses indicate that the thermo-hydrological performance of both the unsaturated zone (UZ) and saturated zone (SZ) will be dominated by repository-heat-driven hydrothermal flow for tens of thousands of years. For thermal loads resulting in extended-dry repository conditions, UZ performance is primarily sensitive to the thermal properties and thermal loading conditions and much less sensitive to the highly spatially and temporally variable ambient hydrologic properties and conditions. The magnitude of repository-heat-driven buoyancy flow in the SZ is far more dependent on the total mass of emplaced spent nuclear fuel (SNF) than on the details of SNF emplacement, such as the Areal Power Density [(APD) expressed in kW/acre] or SNF age.

INTRODUCTION

The Yucca Mountain Site Characterization Project (YMP) of the U.S. Department of Energy (DOE) is investigating the suitability of the fractured, tuffaceous rocks occurring in the unsaturated zone (UZ) at Yucca Mountain, Nevada, for high-level nuclear waste storage. Prior to 1991, efforts in hydrological performance assessment modeling largely focused on either far-field infiltration under ambient conditions or hydrothermal flow in the near-field waste package (WP) environment. Numerical modeling studies have predicted the time-dependent temperature distribution within the emplacement boreholes or drifts and surrounding host rock for various repository design concepts, thermal loading conditions, and waste receipt and operating scenarios.[1,2] These studies involve either finite-element codes of thermal radiation and heat conduction or spatial and temporal superposition of heat conduction calculations to account for the emplacement of individual heat sources over the operational life and post-closure performance of the repository. Because these models do not account for fluid phase changes or heat transfer mechanisms other than thermal radiation or heat conduction, they cannot be used to explicitly predict dry-out performance. On the basis of the assumption that temperatures greater than the nominal boiling temperature (T_b) correspond to the absence of liquid water, the heat conduction models have been used to estimate the minimum time that WPs remain dry.

Nitao considered details of temperature, saturation, and gas-phase composition in the hydrothermally disturbed zone using a model that assumed the repository to be infinite in areal extent.[3] Using a model that averages the repository heat load over a 3-km-diameter disk, Tsang and Pruess conducted repository-scale calculations with an emphasis on thermally driven natural convection.[4] Using a similar 3-km-diameter, disk-shaped model of the repository, we considered a suite of repository-scale calculations, examining the hydrothermal response of the UZ to radioactive heat of decay for 200,000 yr resulting from Areal Power Densities (APDs) ranging from 20 to 114 kW/acre for 30- and 60-yr-old spent nuclear fuel (SNF).[5] Smaller disk-shaped repository areas were also modeled. Calculations were made with a drift-scale model representing the actual dimensions and spacings of drift-emplaced WPs and the emplacement drifts in order to examine the differences between the detailed boiling and dry-out performance of the near-field with the averaged performance predicted by the repository-scale model. The drift-scale model assumed an areally infinite repository with regularly spaced emplacement drifts. The repository-scale model calculations showed that edge-cooling effects at the repository perimeter affected temperatures and saturations in the outer third of the repository area. For the inner two-thirds, the temperature and saturation histories were effectively those of an areally infinite repository. Consequently, the drift-scale calculations were found to be applicable to the inner two-thirds of the repository area.

Our previous work[5] showed the duration of boiling conditions, t_{bp}, to be primarily dependent on the Areal Mass Loading (MTU/acre) of the repository and is much less sensitive to SNF age. For an APD of 114 kW/acre and 60-yr-old SNF, we calculated t_{bp} = 10,000 yr at the center of the repository, with t_{bp} = 5000 yr at the outer edge of the repository. We also found that boiling can result in a dry-out zone extending 300 m vertically (200 m above and 100 m below the repository horizon) and re-wetting of the repository horizon back to ambient conditions requiring 200,000 yr.

It is important to note that our previous work[5] assumed the water table to be at a fixed depth and at a constant temperature, causing the saturated zone (SZ) to act both as a heat sink and as a reservoir for re-wetting the dry-out zone. In this report we conduct calculations utilizing the same fixed-depth and constant-temperature assumptions for the water table. We also conduct an extensive suite of calculations with a model that explicitly represents hydrothermal

flow in the upper 1000 m of the SZ in order to examine the impact of our previous assumptions about the water table. In addition to investigating the impact of SZ heat flow on hydrothermal performance in the UZ, we also examine the impact of repository-heat-driven hydrothermal flow on the thermo-hydrologic performance of the SZ.

This report describes our modeling of the hydrothermal response of the UZ and SZ to the radioactive heat of decay for 200,000 yr for APDs ranging from 20 to 114 kW/acre and 30- and 60-yr-old SNF with a burnup of 33,000 megawatt-days per metric ton of heavy initial metal (MWd/MTU). Two extreme SNF selection scenarios were also considered with the "oldest fuel first" (OFF) scenario yielding an average fuel age and burnup of 26 years and 39,585 MWd/MTU and the "youngest fuel first" (YFF) scenario yielding an average fuel age of 21 years and burnup of 43,573 MWd/MTU. Our models include boiling and condensation effects, the convection of latent and sensible heat, and thermal radiation. The implications of repository-heat-driven hydrothermal flow on site suitability/characterization, total system performance, and in situ testing are discussed.

Overview of Unsaturated Zone Hydrology at Yucca Mountain

Yucca Mountain consists of a series of variably fractured, nonwelded to densely welded tuff units with an eastward tilt of 5 to 30 deg.[6] The UZ thickness varies from 500 to 750 m. The potential repository location is in Topopah Spring (TSw2) moderately to densely welded tuff, which is about 350 m below the ground surface and 225 m above the water table.[7] Montazer and Wilson report the absence of perennial streams at Yucca Mountain.[6] Therefore, recharge due to rainfall or snowmelt occurs episodically.

The matrix properties of the hydrostratigraphic units at Yucca Mountain are summarized by Klavetter and Peters.[7] The units generally fall into two categories: (1) the welded tuffs (TCw, TSw1, TSw2, and TSw3) and the nonwelded zeolitized unit (CHnz), all of which have low matrix permeability, k_m, and low-to-medium matrix porosity, ϕ_m, and (2) nonwelded vitric tuffs of high k_m and ϕ_m (PTn and CHnv). The welded PPw has medium k_m and ϕ_m. The k_ms of the nonwelded vitric tuffs are 4 to 5 orders of magnitude greater than those of the welded tuffs and the CHnz.

Infiltration at Yucca Mountain has been modeled with a one-dimensional steady-state equivalent continuum model (ECM) for recharge fluxes of 0, 0.045, and 0.132 mm/yr, resulting in repository horizon saturations of 68, 85, and 95%, respectively (Fig. 1).[8] On the basis of the assumption of instantaneous capillary pressure equilibrium between fracture and matrix, the ECM volume-averages the fracture and matrix into an equivalent (or effective) continuum. Saturation values obtained from the Reference Information Base (RIB) are also included in Fig. 1.[9] Notice the good agreement between the saturation profile calculated for zero recharge flux and the RIB values in the low-k_m units (TCw, TSw1, TSw2, TSw3, CHnz, and PPw). The RIB values are significantly higher than the calculated profile for the high-k_m units (PTn and CHnv). The saturation profile in the small-k_m units is very sensitive to variations in recharge flux. Because of their large k_m, the PTn and CHnv can sustain a relatively large steady-state recharge flux at small saturations. Nonequilibrium fracture flow through the TCw, TSw1, TSw2, and TSw3 is a likely cause for the apparent inconsistency between the RIB data in the PTn and CHnv and the saturation profile predicted by the one-dimensional, steady-state ECM.[8]

Nitao[10] found that the flow behavior of a two-dimensional, unsaturated fracture-matrix system is characterized by a critical flux, q_f^*, given by

$$q_f^* = \phi_m(S_s - S_i)D_m \quad (1)$$

where ϕ_m is the matrix porosity, S_s is the maximum matrix saturation, S_i is the initial matrix saturation, and D_m is the matrix imbibition diffusivity coefficient. If the flux q_f into the fracture satisfies $q_f \gg q_f^*$, the flow field is fracture-dominated, whereas if $q_f \ll q_f^*$, the flow field is matrix-dominated and the system behaves as a single equivalent porous medium with capillary equilibrium between fracture and matrix. If the fracture entrance is ponded, the critical fracture hydraulic conductivity K_f^*, or corresponding critical aperture b^* from the "cubic" law, controls the flow behavior instead of the critical flux. Rocks with fracture aperture b sufficiently large such that $b^3 \gg b^{*3}$ have fracture-dominated flow, while rocks with fracture aperture sufficiently small such that $b^3 \ll b^{*3}$ are matrix-dominated.

Numerous performance assessment calculations have been carried out for the potential Yucca Mountain repository site. Most of these have utilized a steady-state ECM that, for the assumed recharge fluxes, effectively constrains flow to be matrix-dominated.[8,10] Because of the very low k_m prevalent through most of the UZ, the steady-state ECM calculations have repeatedly shown that matrix-dominated flow will not result in significant vertical transport of radionuclides. Moreover, field evidence indicates that fracture-dominated flow can occur to considerable depth.[11] Therefore, fracture-dominated flow is the only credible mechanism capable of bringing water to the WPs and transporting radionuclides to the water table. The impact of repository-heat-driven hydrothermal flow on fracture-dominated flow is critical to repository performance.

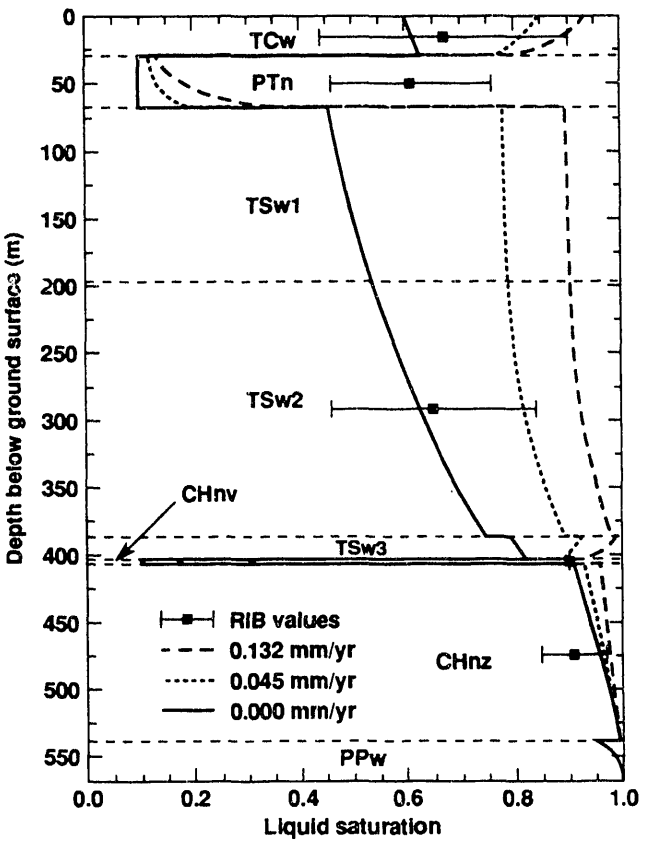

Figure 1. ECM-calculated liquid saturation profile for various steady-state, one-dimensional recharge fluxes vs data from the Reference Information Base (RIB).[7]

Given that liquid flow along preferential fracture flow paths provides the most likely means of generating adverse WP conditions and transporting radionuclides to the water table, three general features or mechanisms tend to mitigate the potential release and transport of radionuclides. The first is discontinuity in preferential fracture flow paths. The second is liquid-phase dispersion in fracture networks, which results as flow branches from a preferential fracture pathway into lateral fractures. The third mechanism is fracture-matrix interaction. For thermal loading conditions that result in sub-boiling conditions, the predominant mode of fracture-matrix interaction is capillary-driven fracture-to-matrix flow, called matrix imbibition. For APDs resulting in marginal boiling conditions, the variability in the heat generation rate among the WPs may result in condensate flow from hotter to cooler WPs, increasing the adverse effects of fracture flow. For higher APDs, boiling effects and enhanced imbibition resulting from rock dry-out will significantly add to the capacity of the UZ to retard fracture-dominated flow.

The characterization and assessment of fracture flow retardation under sub-boiling or ambient conditions in the UZ at Yucca Mountain are extremely formidable. The main problems arise from the very strongly nonlinear dependence of fracture flow on the highly heterogeneous distribution of fracture and matrix properties, uncertainty in characterizing net recharge flux under either current or future (wetter) climate conditions, and the impracticality of incorporating the complex details of variable aperture fracture networks in numerical models. The travel time for a wetting front traveling down a fracture varies inversely with b^6, where b is the fracture aperture.[8] Moreover, the contrast between fracture and matrix permeability can exceed ten orders of magnitude.

For higher APDs, a large region of above boiling conditions makes fracture flow at the repository horizon extremely unlikely. Therefore, under long-term above-boiling conditions, hydrologic performance is governed by the system's thermal loading conditions and thermal properties. These factors can be more readily determined and are much less variable than are many of the parameters associated with the ambient hydrogeological system. Moreover, because the liquid flux associated with condensate generation is found to be much greater than net recharge fluxes associated with pluvial climate conditions, hydrologic performance under long-term above-boiling conditions is much less sensitive to climatic variability. Because the thermal diffusivity is much larger than the re-wetting diffusivity of most of the UZ, temperature tends to equilibrate back to ambient conditions much more quickly than does matrix saturation. Consequently, the matrix saturation within the dry-out zone extending above and below the repository horizon will remain below ambient long after boiling has ceased. Sub-ambient matrix saturations will add to the capacity of the UZ to retard fracture flow during the post-boiling-period.

Hydrothermal Flow at the Repository Horizon

Much of our current understanding of repository-heat-driven hydrothermal flow in unsaturated fractured tuff is based on observations made during the heater tests in G-Tunnel[12] and associated modeling studies.[13,14] For drift emplacement without backfill, the primary mode of heat transfer from the WP to the wall of the emplacement drift is thermal radiation (Fig. 2). If backfill is present, heat flow through the backfill will be dominated by heat conduction.

Both the G-Tunnel heater test modeling analysis[14] and the performance analysis of repository-heat-driven hydrothermal flow[5] have indicated that heat flow in the UZ will be dominated by heat conduction. Because of the large bulk permeability of fracture networks, gas-phase pressures, p_g, in the fractures remain very close to atmospheric, even during boiling. Consequently, as temperatures reach the nominal boiling point ($T_b \approx 96$°C), boiling first occurs along the fracture faces, i.e., the perimeter of the matrix blocks, and proceeds in toward the center of the matrix blocks. Because of the small k_m at the repository horizon, boiling results in large p_g gradients (with p_g increasing from the perimeter to the center of the matrix blocks), causing a rise in the boiling temperature, ΔT_b, above the nominal boiling point, T_b. Because p_g gradients increase with matrix block size, ΔT_b increases with matrix block size. Accordingly, boiling is more suppressed in sparsely fractured regions and less suppressed in intensely fractured regions. For regularly spaced fractures, the volume of the dry-out zone was found to be proportional to $\sqrt{k_m}/B$, where B is the effective fracture spacing.[14] For the G-Tunnel test, B was apparently small enough (relative to k_m) that the effect of ΔT_b on rock dry-out was negligible. The sensitivity of the dry-out volume to fracture aperture, b, was also examined.[14] For $b > 20$ μm, the volume of the dry-out zone was found to be insensitive to b. For the fractures observed in G-Tunnel, flow resistance in the fractures does not appear to throttle the rate of dry-out.

At early time, a small percentage of the water vapor that reaches the fracture network in the immediate vicinity of the WP flows back toward the emplacement drift (Fig. 2). Otherwise, most of the water vapor reaching the fracture network is driven (by higher p_gs in the boiling zone) away from the emplacement drift to where cooler temperatures cause it to condense along fracture walls. Because the small k_m limits the rate of matrix imbibition, condensate drainage down fractures persists for considerable distances before being imbibed by the matrix. In the region below the boiling zone, condensate drainage is away from the boiling front (Fig. 2), enhancing the rate of rock dry-out. Above the boiling zone, condensate tends to drain back toward the boiling zone, thereby retarding the net rate of dry-out (Fig. 2).

During the G-Tunnel test, regions above the heater were observed to dry out more slowly than regions below the heater.[12] Because vapor flow in fractures tends to be radially away from the

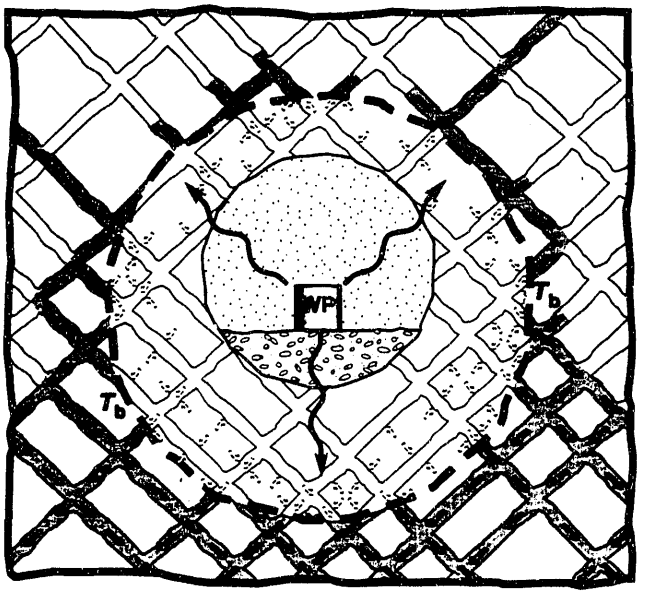

Figure 2. Schematic of hydrothermal flow near the emplacement drift. Rock dry-out occurs as boiling drives water vapor out of the rock matrix. Upon reaching the fracture network, vapor is driven away from the boiling zone to where cooler temperatures cause it to condense along fracture walls. Because the small k_m limits the rate of matrix imbibition, condensate drainage persists for considerable distances down fractures.

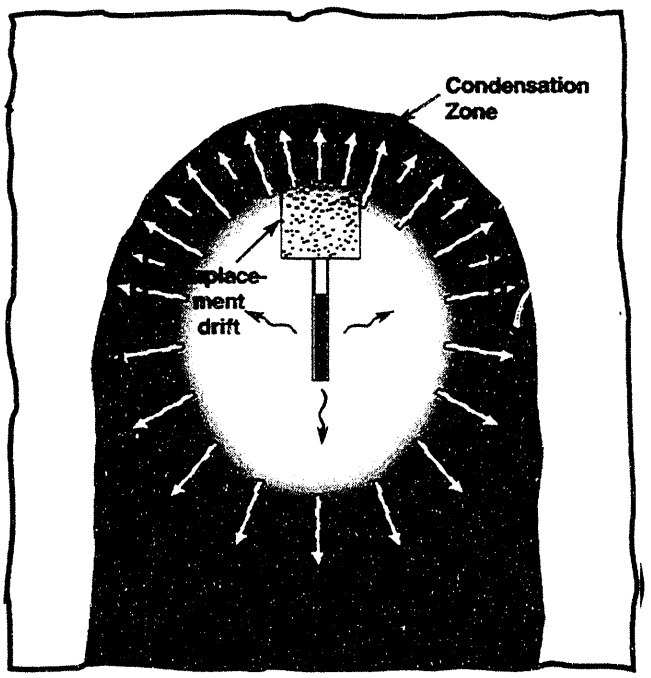

Figure 3. A "hydrothermal umbrella" is established along each of the emplacement drifts because of condensate being shed off the top and down the sides of the boiling zone.

heat source and condensate drainage is vertically downward, successive refluxing cycles in fractures eventually result in condensate being shed off the top and down the sides of the boiling zone (Fig. 3). This "hydrothermal umbrella" effect was manifested during the G-Tunnel test in the temperature history of several thermocouples along the flank of the boiling zone. This concept was first mentioned by Roseboom in the context of emplacing high-level nuclear waste in the UZ.[15] The "umbrella" mechanism may significantly enhance near-field dry-out, at least until the dry-out zones of neighboring emplacement drifts (or panels) have coalesced.

DISCUSSION OF NUMERICAL MODELS, PHYSICAL DATA, AND ASSUMPTIONS

V-TOUGH Hydrothermal Flow Code

All hydrothermal calculations in this study were carried out using the V-TOUGH ("vectorized transport of unsaturated groundwater and heat") code.[16] V-TOUGH is Lawrence Livermore National Laboratory's enhanced version of the TOUGH code, which is a member of the Mulkom family of multiphase, multicomponent codes developed at Lawrence Berkeley Laboratory by Pruess.[17] V-TOUGH is a multidimensional numerical simulator capable of modeling the coupled transport of water, vapor, air, and heat in fractured porous media.

Equivalent Continuum Model

Because of the impracticality of discretely accounting for all of the fractures within the repository block, it was necessary to account for fractures using the ECM. The assumption of capillary pressure and thermal equilibrium between fractures and matrix allows the fracture and matrix properties to be pore-volume-averaged into an equivalent medium. The bulk porosity, ϕ_b, bulk saturation, S_b, and bulk hydraulic conductivity, K_b, of the equivalent medium are given by:

$$\phi_b = \phi_f + (1-\phi_f)\phi_m \tag{2}$$

$$S_b = \frac{S_f\phi_f + S_m(1-\phi_f)\phi_m}{\phi_f + (1-\phi_f)\phi_m} \tag{3}$$

$$K_b = K_m(1-\phi_f) + K_f\phi_f \tag{4}$$

where ϕ_m, S_m, ϕ_f, and S_f are the porosity and saturation of the matrix and fractures, respectively. Because of the small K_m in the UZ, K_b is almost completely dominated by K_f and ϕ_f for most fracture spacings and permeabilities.

In general, the ECM is appropriate for situations in which the fracture spacing is small enough to result in a negligible lag in the wetting or drying response in the matrix relative to that of the fractures. The use of the ECM implicitly assumes that flow resistance to liquid and vapor flow between the fractures and matrix is negligible. In the modeling analysis of the G-Tunnel heater test, the ECM-calculated saturation profile compared very well with the measured saturation in the dry-out zone.[14] Apparently, the fracture spacing was sufficiently small so that, during boiling, the resistance to vapor flow from matrix to fracture was negligible. Although the ECM predicted a pronounced rise in liquid saturation in the condensate zone, the G-Tunnel data showed no significant rise in liquid saturation outside of the boiling zone. With respect to matrix imbibition of condensate, the fracture spacing was not sufficiently small to validate the assumption of capillary pressure equilibrium in the condensate zone. Moreover, the lack of a rise in liquid saturation outside of the boiling zone, as well as some of the temperature data along the side of the boiling zone, indicated the "hydrothermal umbrella" effect of condensate shedding off the top and down the sides of the boiling zone.

The ECM-calculated temperature profile agreed very well with the measured G-Tunnel data.[14] This close agreement was also obtained for a model that only accounted for heat conduction, indicating that heat flow around the G-Tunnel heater was dominated by heat conduction. On the basis of the G-Tunnel model validation effort, and given the similarity between the fracture and matrix properties of Grouse Canyon welded tuff in G-Tunnel and the Topopah Spring welded tuff at the repository horizon, the ECM should yield accurate predictions of temperature performance and conservatively low predictions of the spatial extent and duration of rock dry-out. In light of the capillary hysteresis effect observed for Grouse Canyon welded tuff,[13,18] the ECM-calculated time required to re-wet the dry-out zone may be considerably less than actual.

Thermo-Hydrologic Properties

All major hydrostratigraphic units in the UZ at Yucca Mountain are included in the models.[7,19] This hydrostratigraphic profile has been used in previous modeling studies.[5,8] The wet and dry thermal conductivity, K_{th}, data were obtained from the RIB.[9] In previous hydrothermal calculations, RIB Version 3 K_{th} values were used.[5,14] In this study we use the RIB Version 4 K_{th} values. Calculations for various repository thermal loads were repeated for initial saturation conditions corresponding to the steady-state saturation profiles obtained by Buscheck, Nitao, and Chesnut[8] for net recharge fluxes of 0 and 0.132 mm/yr, which resulted in repository horizon saturations of 68 and 95%, respectively (Fig. 1). Previous work[5] also considered the steady-state saturation profile obtained for a net recharge flux of 0.045 mm/yr, resulting in a repository horizon saturation of 85%. This range in initial steady-state saturation distribution should adequately span the range in saturation conditions that could arise from extreme pluvial climatic conditions.

The reference case assumed a bulk permeability, k_b, of $2.8 \times 10^{-13} m^2$ (three 100-μm fractures per meter). The sensitivity of boiling and dry-out performance to k_b was examined by considering $k_b = 1.9 \times 10^{-18} m^2$ (no fractures). Previous work[5] also considered $k_b = 1.0 \times 10^{-11} m^2$ (approximately three 346.5-μm fractures per meter) and $k_b = 8.3 \times 10^{-10} m^2$ (one 1000-μm fracture per meter).

Initial and Boundary Conditions

The vertical temperature, T, distribution in the models is initialized to correspond to the nominal geothermal gradient in the region. The atmosphere at the ground surface is represented by a constant-property boundary, with T and p_g fixed at 13°C and 0.86 atm, respectively. The relative humidity at the ground surface is also fixed so that it is in capillary equilibrium with the initial saturation conditions at the top of the TCw unit. Therefore, under initial (ambient) saturation and temperature conditions there is no mass flux of water vapor between the atmosphere and upper TCw. In previous work[5] it was assumed that because of the large fracture permeability, buoyancy-driven convective mixing in the SZ results in the SZ acting as a heat sink. The large bulk permeability and storativity of the SZ is also assumed to result in the water table being at a fixed depth. For some of the calculations in this report we also assume that the water table has a fixed depth ($z = 568.1$ m) and a constant temperature (31°C). The fixed-depth water table assumption causes the SZ to effectively act as an infinite reservoir of liquid water for re-wetting the dry-out zone. The constant-temperature water table assumption causes the water table to act as a heat sink. Consequently, these assumptions are conservative with respect to predictions of the extent and duration of boiling conditions and rock dry-out effects. Because this model does not explicitly model hydrothermal flow in the SZ, it is called the "UZ" model. The initial temperature and saturation at the repository horizon in the UZ model are 23.3°C and 68%, respectively.

The geothermal gradient was found to result in a two-phase recirculation of vapor and liquid water in the UZ.[5] For both the previous study[5] and this study, the reference case assumes an initial saturation distribution that arises from a 0 mm/yr one-dimensional steady-state recharge flux (Fig. 1). Note that the recharge flux values listed in Fig. 1 are the net downward moisture flux. Because of the relative humidity gradients that result from the natural geothermal gradient, a 0 mm/yr net moisture flux turns out to be the net effect of an upward flux of water vapor that condenses and is balanced by an equivalent downward flux of liquid water. At the repository horizon, this steady-state counter-current flow system results in a downward liquid flux of 0.01 mm/yr. Although low APDs do not result in significant boiling effects, the repository heat is sufficient to significantly increase the vertical temperature gradient, thereby enhancing the counter-current flow of vapor and liquid water. The repository-heat-driven downward flux of condensate may be large relative to the net recharge flux under ambient conditions.

A fundamental objective of this study was to establish the spatial domain over which the thermo-hydrological performance of the engineered and natural barriers is critically dependent. Because model boundaries generally have assigned property values such as pressure and temperature or assigned fluxes, it is important to determine whether these boundaries are located sufficiently far from the repository heat source so that they do not artificially interfere with the thermo-hydrological performance of the engineered and natural barriers. Because of the large magnitude of convective mixing in the atmosphere, we felt that assigning a constant-property boundary at the ground surface was reasonable. However, we felt it was necessary to test the assumption that sufficient buoyancy-driven convective mixing occurs in the SZ to result in the water table functioning as a heat sink. Moreover, if SZ buoyancy-driven convective mixing is sufficient to result in the water table functioning as a heat sink, then those same convective effects should also dramatically affect the performance of the natural barriers in the SZ.

We conduct a suite of calculations with a "UZ-SZ" model (which includes hydrothermal flow in the upper 1000 m of the SZ) and compare those calculations with those of the "UZ" model in order to directly assess the impact of assuming a fixed-depth, constant-temperature water table. Conductive and convective heat flow, including buoyancy flow, are modeled in the SZ. Because the RIB[9] lacks thermal property and hydrologic data below the PPw unit (the lowermost hydrostratigraphic unit in our UZ model), we assumed that the PPw data was applicable to the upper 1000 m of the SZ (down to the lower boundary of the UZ-SZ model). The lower boundary of the UZ-SZ model has a constant temperature of 53.5°C and a fixed pressure corresponding to the hydrostatic pressure and temperature profile of the upper 1000 m of the SZ. The initial temperature and saturation at the repository horizon in UZ-SZ model is 23.5°C and 67.7%, respectively. As will be discussed later, we find that buoyancy-driven convective mixing in the SZ is not sufficient to cause the water table to function as a heat sink. Accordingly, we conduct much of this study, particularly those sub-sections which examine the sensitivity of thermo-hydrological performance to thermal loading conditions, with the UZ-SZ model (which includes hydrothermal flow in the SZ).

For a 1747-acre repository, the repository-scale model represents the repository as a 3-km-diameter, 4.6-m-thick, disk-shaped heat source with a uniformly distributed thermal load. Repository areas of 348, 559, 1118, and 3162 acres were also modeled. The model utilizes an axisymmetric coordinate system centered at the repository center. This model is useful for calculating temperature and saturation behavior (averaged from one emplacement drift to the next) as a function of location relative to the center (or edge) of the repository area. The assumption is also made that the thermal loading of the repository can be represented by the heat generation curve of pressurized water reactor (PWR) spent fuel of an average age. Calculations were made for APDs ranging from 20 to 114 kW/acre and SNF ages of 30 and 60 yr with a burnup of 33,000 MWd/MTU. Two extreme SNF selection scenarios were also considered with the "oldest fuel first" (OFF) scenario yielding an average fuel age and burnup of 26 years and 39,585 MWd/MTU and the "youngest fuel first" (YFF) scenario yielding an average fuel age of 21 years and burnup of 43,573 MWd/MTU.

DISCUSSION OF MODELING RESULTS

Overview of the Parameter Sensitivity Study

In this section, we examine the sensitivity of thermo-hydrological performance in the unsaturated zone (UZ) and saturated zone (SZ) to a range of (1) thermal loading design parameters and (2) thermo-hydrological properties and boundary conditions. The first four sub-sections address the sensitivity of thermo-hydrologic performance to thermal loading parameters with the use of the UZ-SZ model and "reference case" properties and conditions described in the previous section. The following five sub-sections address the sensitivity of thermo-hydrological performance to thermo-hydrological properties and boundary conditions. On the basis of the analysis of the sensitivity of thermo-hydrological performance to thermo-hydrological properties, we feel that the UZ-SZ model with the reference properties and conditions is the best model for representing large-scale repository performance. We feel that this model is particularly useful for high thermal loads resulting in long-term boiling conditions at the repository horizon.

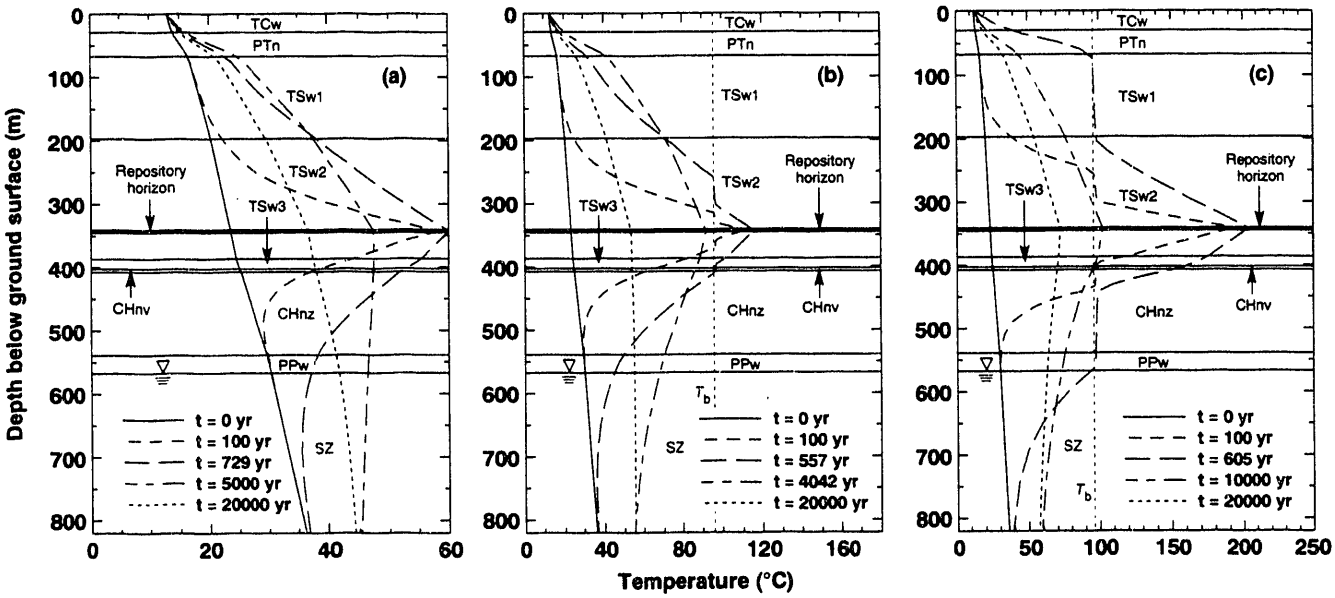

Figure 4. Vertical temperature profiles along the repository centerline for 30-yr-old SNF, a net recharge flux of 0 mm/yr, and APDs of (a) 20 kW/acre, (b) 57 kW/acre, and (c) 114 kW/acre.

The tenth sub-section examines the sensitivity of thermo-hydrological performance in the SZ to thermal loading design parameters as well as the thermo-hydrological properties. The eleventh and final sub-section summarizes thermo-hydrological performance with the use of major hydrothermal flow regimes.

For this study, we focus much of our attention on the temperature history at the repository horizon because of its importance to WP integrity, potential release, and transport of radionuclides. As will be shown, it is likely that we can reliably predict the thermal performance at the repository horizon (particularly for high thermal loadings). The ability of reliably predicting the duration of boiling conditions in the vicinity of WPs will be extremely useful in determining the duration of time that WP failure, radionuclide release and transport is very unlikely because of the lack of liquid water.

Temperature Profiles as a Function of Thermal Load

The next four sub-sections examine the sensitivity of thermo-hydrological performance to thermal loading design parameters. We begin our investigation with a look at the vertical temperature profile in the UZ and SZ for three thermal loading cases covering a broad range in thermal loading conditions and thermo-hydrological performance. Note, that because our model homogenizes the thermal load over the repository area, predicted temperatures should be considered to be "averaged" temperature conditions (particularly at the repository horizon). The effect of spatially averaging the thermal load over the repository area has a diminishing effect on temperatures with increasing distance from the repository horizon. The effect of spatially averaging the thermal load also diminishes with time. Therefore, there may be significant differences between detailed temperature behavior (e.g., in the pillar separating WP emplacement drifts) and the average temperature predicted for the repository. On the other hand, locations far out in the natural barriers feel the effects of the average thermal loading conditions rather than the discrete details of the heat load distribution. The three cases considered in this subsection include a "sub-boiling" case, a "marginal-boiling" case, and a "long-term, extended-dry" case.

For 30-yr-old SNF and a recharge flux of 0 mm/yr, the vertical temperature profile along the repository centerline is plotted for APDs of 20, 57, and 114 kW/acre (Fig. 4a–c). The ground surface is located at $z = 0$ m, the repository horizon is centered at $z = 343.1$ m, and the water table is located at $z = 568.1$ m below the ground surface (225 m below the repository horizon). Notice that the water table begins to experience a temperature buildup, ΔT, at $t = 100$ yr. Even for 20 kW/acre, ΔT at the water table is substantial, persisting for tens of thousands of years (Fig. 5a). For 20 kW/acre, the water table peaks at 46.9°C (ΔT = 16.5°C) at $t = 6900$ yr and remains above 40°C for 26,350 yr (Fig. 5a). For 114 kW/acre, the water table peaks at 95°C at $t = 830$ yr, remains above 90°C for 670 yr, and remains above 70°C for 12,400 yr. Even 250 m below the water table (475 m below the repository center), ΔT is quite substantial (Fig. 5b), with the maximum ΔT, ΔT_{max}, at this depth being 10.8, 21.6, and 22.9°C for APDs of 20, 57, and 114 kW/acre, respectively.

We have included the reference Site Characterization Plan – Conceptual Design Report[20] (SCP-CDR) case (APD=57 kW/acre; 10-yr-old SNF) in Fig. 5a and b in order to illustrate that the reference SCP-CDR thermal load very substantially alters the temperature of the natural barriers both within the unsaturated zone (UZ) and the saturated zone (SZ). For the reference SCP-CDR thermal load, ΔT_{max} at the water table is 29.8°C, occurring at $t = 4140$ yr. At a depth of 250 m below the water table (475 m below the center of the repository), ΔT_{max} is 19.5 °C, occurring at $t = 8390$ yr (Fig. 5b). Approximately one-third of the way into the CHnz unit (106.5 m below the center of the repository), $\Delta T_{max} = 45.4$°C, occurring at $t = 1635$ yr. At $t = 20{,}000$ yr, ΔT at this location in the CHnz is 21.1°C.

Such a substantial, persistent increase in temperature has the potential for driving geochemical alteration (such as mineral dissolution and precipitation along fractures), resulting in significant changes to the flow and transport properties of potential pathways for radionuclide transport in the UZ and SZ. Our calculations also show considerable condensate drainage in the UZ below the repository, driven by the reference SCP-CDR thermal load. For vertically connected preferential fracture pathways, our calculations indicate that repository-

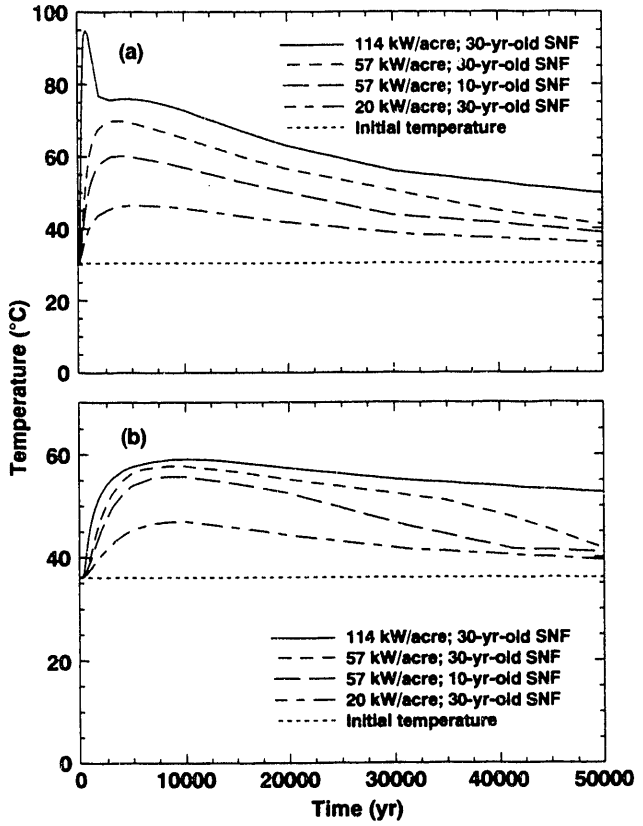

Figure 5. Temperature history at locations below the repository center for various thermal loading conditions, including (a) the water table and (b) 250 m below water table.

heat-driven condensate drainage can persist all the way to the water table. Condensate drainage along fractures may also contribute to the alteration of flow and transport properties in the natural barriers underlying the repository.

Recall that previous hydrothermal calculations[5] assume that the water table is at a fixed depth and constant temperature. Moreover, several of the repository thermal studies involving heat conduction models also make the same assumption.[1,2] On the basis of Fig. 5a and b, it is apparent that maintaining a constant temperature at the water table has the effect of artificially constraining the magnitude of ΔT in the lower UZ, particularly in the CHnz and PPw units. Artificially maintaining the water table at a constant temperature will also be shown to significantly limit the duration of elevated temperatures at the repository. Moreover, models that fix the water table temperature cannot be used to assess the potential impacts of temperature rise and repository-heat-driven convective flow in the SZ on radionuclide transport in the SZ.

As will be seen in a following sub-section on hydrothermal flow in the SZ, our UZ-SZ model predicted substantial repository-heat-driven buoyancy flow in the SZ; however, heat flow from the UZ to the SZ does not deviate significantly from being heat-conduction-dominated. We investigated the sensitivity of repository-heat-driven buoyancy flow in the SZ to the bulk permeability, k_b, in the SZ and found that it is extremely unlikely that k_b in the SZ is large enough to result in the water table effectively functioning as a heat sink. Therefore, it is inappropriate to treat the water table as a heat sink. Accordingly, we conducted most of this study with the UZ-SZ model which includes hydrothermal flow in the SZ.

The effects of boiling, steam, and condensate flow are apparent in the 57- and 114-kW/acre cases (Fig. 4b and c). Notice that the temperature profile is flattened at T_b ($\approx$ 96°C). Steam is driven (by higher p_gs in the boiling zone) away from the repository to where cooler temperatures cause it to condense. Above the repository horizon, much of this condensate is driven back to the boiling zone, primarily by three processes: (1) capillary imbibition in the matrix, (2) capillary imbibition in small-aperture fractures, and (3) gravity drainage in fractures. Gravity drainage in the matrix is not significant in comparison with matrix imbibition, which is driven by very large capillary pressure gradients that arise from saturation gradients in the boiling and condensation zones. Below the repository horizon, only the first two mechanisms, capillary-driven flow in the matrix and fractures, contribute to condensate flow back toward the boiling zone, while the third mechanism, gravity drainage in fractures, tends to drain condensate away from the boiling zone.

The return flow of condensate back toward the boiling zone establishes a heat transfer mechanism (driven by the convection of latent heat) called the gravity-driven "heat pipe" effect. Given adequately high mass flux rates of the counter-current flow of steam and condensate, heat pipes are capable of sustaining a given heat flux with a much shallower temperature gradient than is associated with heat conduction. Consequently, heat pipes are manifested by a very flat temperature profile, with temperatures close to T_b (Fig. 4b and c). Mass fluxes associated with gravity-driven fracture flow are much greater than those associated with capillary-driven flow in either the matrix or fractures. Therefore, above the repository, gravity-driven condensate flow in fractures is the predominant source of liquid flow back to the boiling zone. While the flattening of the temperature profile above the repository is primarily attributed to the gravity-driven refluxing or heat pipe effect, the flattening of the temperature profile below the repository is attributed to condensate drainage convecting heat away from the boiling zone.

Classical heat pipes derive much of their thermal efficiency from their working fluid operating within a closed loop. As discussed earlier, the "hydrothermal umbrella" effect causes condensate to shed down the sides of the boiling zone.[5,12,14] The loss of working fluid contributes to the migration of the boiling front away from the heat source because the return flow of condensate cannot keep pace with the rate of vaporization. Incidentally, regardless of whether working fluid is lost, an adequately high heat flux is capable of driving steam away from the heat source faster than the rate at which liquid water can return, thereby causing the dry-out front to advance. Condensate shedding results in a net loss of working fluid from the heat pipe, enhancing the rate at which the boiling front migrates away from the heat source. Because the ECM assumes capillary pressure equilibrium between fracture and matrix, condensate that would have drained freely under nonequilibrium fracture flow conditions is artificially held up in the matrix where it is unable to drain freely away from the boiling zone. Consequently, the ECM tends to underpredict the dry-out rate.

Repository Temperatures as a Function of Thermal Load

While the last sub-section examined the temperature profile throughout the UZ and SZ, this sub-section focuses on the thermal performance at the repository. The temperature history at the repository center is plotted for APDs ranging from 20 to 114 kW/acre, a recharge flux of 0 mm/yr for 30-yr-old SNF (Fig. 6a) and 60-yr-old SNF (Fig. 6b). Notice that the threshold APD for significant boiling effects lies between 36 and 57 kW/acre for 30-yr-old SNF and between 20 and 36 kW/acre for 60-yr-old SNF. Note that the temperature histories (Fig. 6a and b) are for a 1747-acre repository. However, we find that the thermal performance at the repository center is insensitive to repository area (Table 1) for a wide range of

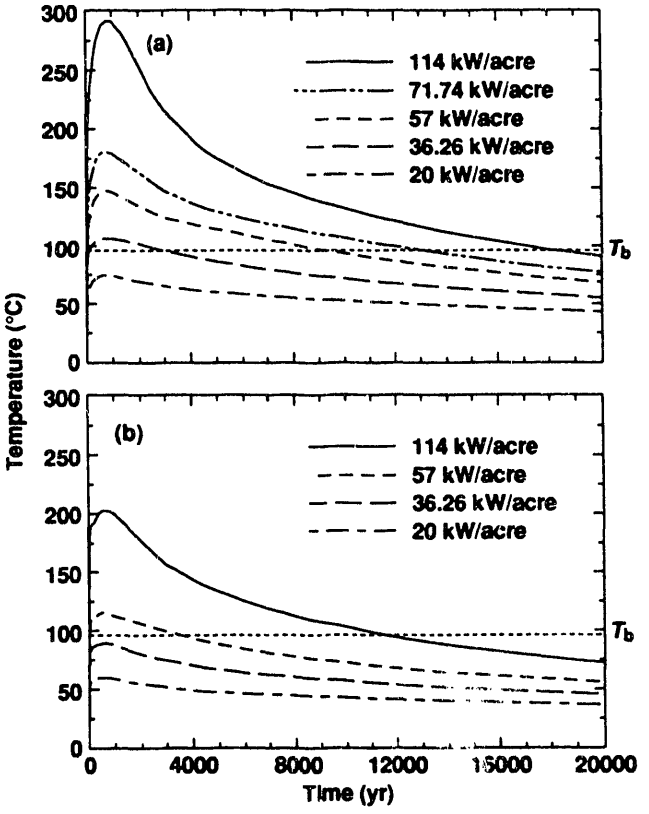

Figure 6. Temperature history at repository center for a net recharge flux of 0 mm/yr, including hydrothermal flow in SZ, for (a) 60-yr-old SNF and (b) 30-yr-old SNF.

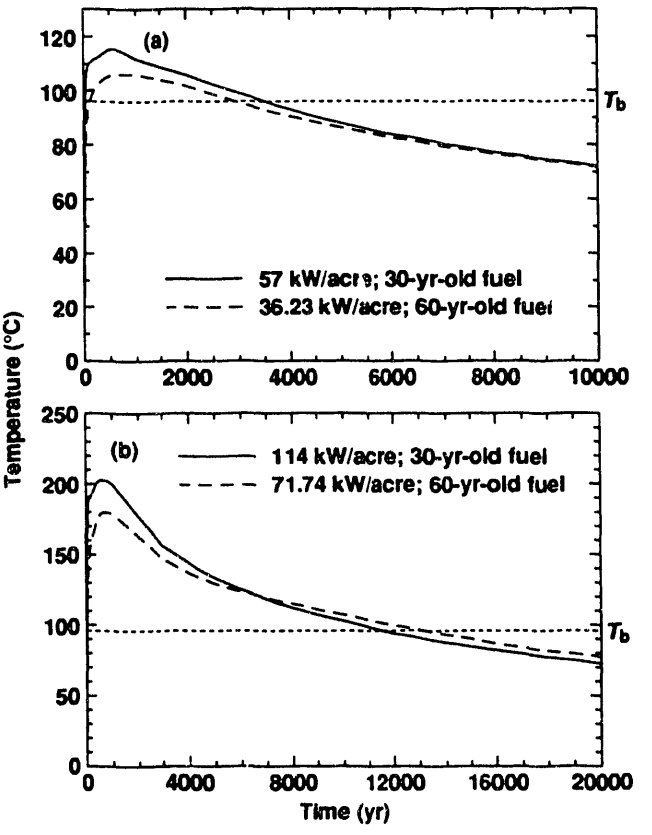

Figure 7. Temperature history at repository center for a net recharge flux of 0 mm/yr, including hydrothermal flow in SZ for an AML of (a) 77.4 MTU/acre and (b) 154.7 MTU/acre.

areas. Therefore, Fig. 6a and b can be considered to be applicable to the range of repository areas listed in Table 1. Thermal performance at the edge of the repository is also found to be insensitive to repository area. Our previous study[5] also found thermal performance at the repository center and edge to be insensitive to repository area. Notice that the time to peak temperature is approximately 600 yr for 30-yr-old SNF and 800 yr for 60-yr-old SNF. Generally, 60-yr-old SNF attains anywhere from 75 to 87% of its ultimate temperature buildup within the first 100 years, while 30-yr-old SNF attains about 94% of its ultimate temperature buildup within the first 100 years.

Repository Temperatures as a Function of Areal Mass Loading

For a given burnup [expressed as megawatt-days per metric ton of initial heavy metal (MWd/MTU)], the most useful macroscopic thermal loading parameter in analyzing long-term thermal performance is the Areal Mass Loading [(AML) expressed in metric tons of uranium per acre, MTU/acre]. We compare cases having the same AML, but different APD and SNF age for a net recharge flux of 0 mm/yr. As was observed in our previous study,[5] the duration of boiling, t_{bp}, is primarily determined by the AML. Notice that for an AML of 77.4 MTU/acre (Fig. 7a), t_{bp} at the repository center is nearly the same, regardless of APD and SNF age. For the APD=57 kW/acre, 30-yr-old SNF case, t_{bp}=3506 yr, while for the APD=36.2 kW/acre, 60-yr-old SNF case, t_{bp}=2931 yr (Table 1). Similarly, for an AML of 154.7 MTU/acre (Fig. 7b), t_{bp} is nearly the same, regardless of APD and SNF age. For the APD=114 kW/acre, 30-yr-old SNF case, t_{bp} is 11,446 yr, while for the APD=71.7 kW/acre, 60-yr-old SNF case, t_{bp}=12,984 yr (Table 1). For a given AML, the peak repository temperature, T_{peak}, for 60-yr-old SNF is significantly lower than for 30-yr-old SNF (Table 1). Generally, early temperature performance (including T_{peak}) is sensitive to SNF age, while t_{bp} and post-boiling-period thermal performance is determined by the AML (and is insensitive to SNF age).

Table 1. Thermal Performance at the Center of a Repository Containing Spent Nuclear Fuel (SNF) with a Burnup of 33,000 MWd/MTU

AML (MTU/acre)	APD (kW/acre)	Area (acres)	SNF age (yr)	$T_{100\,yr}$ (°C)	T_{peak} (°C)	t_{peak} (yr)	t_{bp} (yr)
27.1	20.0	3162	30	57.8	59.9	729	NA
27.1	20.0	1747	30	57.8	59.9	730	NA
43.5	20.0	1747	60	63.7	74.4	667	NA
49.2	36.2	1747	30	85.1	89.2	641	NA
49.2	57.0	1747	10	100.0	100.3	94	666
77.4	36.2	1747	60	95.4	106.0	800	2931
77.4	57.0	1118	30	109.7	115.4	557	3382
77.4	57.0	1747	30	109.7	115.3	601	3506
124.3	57.0	1747	60	122.3	146.8	800	9262
154.7	71.7	1747	60	145.9	179.9	800	12984
154.7	114.0	559	30	191.2	202.9	605	11446
154.7	114.0	1747	30	190.7	202.9	653	10685
248.5	114.0	348	60	225.7	291.5	816	18121

Repository Temperatures as a Function of SNF Burnup

For this report, as in our previous work,[5] all hydrothermal calculations have considered 10-, 30-, and 60-yr-old SNF having the reference SCP-CDR burnup of 33,000 megawatt-days per metric ton of heavy initial metal (MWd/MTU). In order to investigate the thermo-hydrological performance of the repository-UZ-SZ system under repository thermal loads that are more specifically tied to potential SNF selection options for the repository, we conducted calculations for SNF with other average ages and burnups. Two extreme SNF selection scenarios were considered with the "oldest fuel first" (OFF) scenario yielding an average fuel age and burnup of 26 years and 39,585 MWd/MTU, and the "youngest fuel first" (YFF) scenario yielding an average fuel age of 21 years and burnup of 43,573 MWd/MTU. We considered the 21-yr-old OFF and 26-yr-old YFF scenarios for APDs of 20 and 114 kW/acre.

For the 20 kW/acre cases, a 3162-acre repository was considered. For the 21-yr-old YFF scenario, the 26-yr-old OFF scenario, and the 30-yr-old SNF reference case, an APD of 20 kW/acre results in an AML of 16.6, 20.4, and 27.1 MTU/acre, respectively. The 21-yr-old YFF scenario attains a peak average temperature at the repository center, T_{peak}, of 55.5°C at a time to peak temperature, t_{peak}, of 150 yr, while for the 26-yr-old OFF scenario, T_{peak} = 57.9°C at t_{peak} = 236 yr (Table 2 and Fig. 8a). For the 30-yr-old SNF reference case, T_{peak} = 59.9°C at t_{peak} = 729 yr (Table 2 and Fig. 8a). As has been previously observed,[5] t_{peak} increases with average SNF age. Although t_{peak} varies considerably among these three cases, there is very little substantive difference among the respective temperature profiles because most of the temperature buildup occurs during the first 100 years. For example, the 30-yr-old SNF case attains 94% of its ultimate temperature buildup during the first 100 years, with the temperature only increasing another 2.2°C between t = 100 and 729 yr (Table 2 and Fig. 8a). The 21-yr-old YFF and 26-yr-old OFF scenarios attain over 99% of their ultimate temperature buildup during the first 100 years (Table 2 and Fig. 8a). Therefore, although t_{peak} may appear to vary considerably, actual differences in repository temperature at any given time are relatively minor among the three 20 kW/acre cases (Fig. 8a).

It should be emphasized that T_{peak} is the peak averaged temperature at the repository center. Consequently, T_{peak} does not reflect temperature gradients between the emplacement drift wall and the pillar centers, nor does it reflect spatial temperature variations arising from the variability in the heat output among WPs. Because peak temperatures are nearly attained in 100 yr, thermal homogenization will not have had sufficient time to impact local peak temperatures within the repository. Therefore, actual distributions of peak temperature will deviate significantly from the values of T_{peak} given above. Depending on the number of fuel assemblies per WP and variations in the WP heat output, local boiling conditions can persist for hundreds of years even if average repository temperatures might appear to be indicative of sub-boiling conditions. If WPs contain more than two PWR fuel assemblies, local boiling conditions appear to be likely.

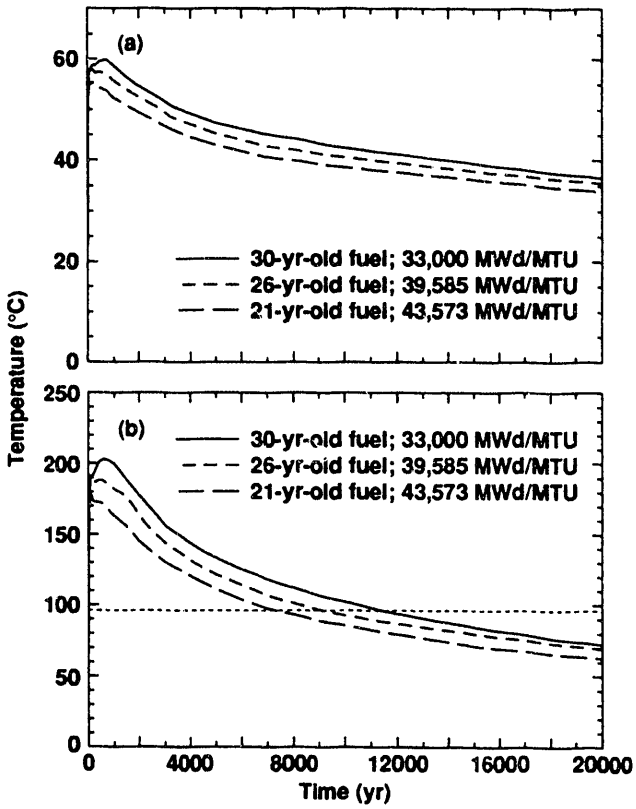

Figure 8. Temperature history at repository center for a net recharge flux of 0 mm/yr, including hydrothermal flow in the SZ. (a) APD = 20 kW/acre and a 3162-acre repository. (b) APD = 114 kW/acre and a 559-acre repository.

For the 114 kW/acre cases, a 559-acre repository was considered. For the 21-yr-old YFF scenario, the 26-yr-old OFF scenario, and the 30-yr-old SNF reference case, an APD of 114 kW/acre results in AMLs of 94.7, 116.5, and 154.7 MTU/acre, respectively. For the 21-yr-old YFF scenario, T_{peak} = 177.5°C at t_{peak} = 122 yr. For the 26-yr-old OFF scenario, T_{peak} = 188.2°C at t_{peak} = 454 yr. For the 30-yr-old SNF case, T_{peak} = 202.9°C at t_{peak} = 605 yr. Although t_{peak} varies considerably among these three cases, all three cases are effectively at their peak temperature within the first 100 yr (Table 3 and Fig. 8b). For the 21-yr-old YFF and 26-yr-old OFF cases, over 99% of the ultimate temperature buildup occurs during the first 100 yr, while 94% of the ultimate temperature buildup occurs for 30-yr-old SNF case during the first 100 yr, with temperature only rising another 11.6°C between t = 100 and 602 yr (Table 3 and Fig. 8b).

Table 2. Thermal Performance at the Center of a 3162-Acre Repository With an APD of 20 kW/acre

AML (MTU/acre)	Burnup (MWd/MTU)	IED (GWd/acre)	SNF age (yr)	$T_{100\ yr}$ (°C)	T_{peak} (°C)	t_{peak} (yr)	t_{bp} (yr)
16.6	43573	723	21	55.3	55.5	150	NA
20.4	39585	808	26	57.0	57.9	236	NA
27.1	33000	894	30	57.8	59.9	729	NA

Table 3. Thermal Performance at the Center of a 559-Acre Repository With an APD of 114 kW/acre

AML (MTU/acre)	Burnup (MWd/MTU)	IED (GWd/acre)	SNF age (yr)	$T_{100\ yr}$ (°C)	T_{peak} (°C)	t_{peak} (yr)	t_{bp} (yr)
94.7	43573	4126	21	177.3	177.5	122	7[illegible]31
116.5	39585	4612	26	187.1	188.2	454	[illegible]5
154.7	33000	5105	30	191.2	202.9	605	1 [illegible]3

The Integral Energy Density [(IED) expressed in GWD/acre] is an important macroscopic parameter in evaluating long-term thermo-hydrological performance. IED is obtained from the product of AML and burnup. For the 21-yr-old YFF scenario, the 26-yr-old OFF scenario, and the 30-yr-old SNF reference case, an APD of 114 kW/acre results in IEDs of 4126, 4612, and 5105 GWd/acre, respectively (Table 3). In our previous study,[5] t_{bp} was found to scale as the $IED^{1.5}$. For the three 114 kW/acre cases in this sub-section, we found t_{bp} scales as the $IED^{2.1}$. For the 21-yr-old YFF scenario, the 26-yr-old OFF scenario, and the 30-yr-old SNF reference case, t_{bp} is 7331, 9125, and 11,446 yr, respectively (Table 3 and Fig. 8b). Had we assigned equal IED (rather than equal APD) to these three scenarios, t_{bp} would have been similar for the three SNF ages, with the 21-yr-old YFF case having the highest T_{peak}. Because of the relatively large t_{bp}, thermal homogenization within the repository will have occurred prior to the end of the boiling period. Therefore, spatial variability in heat output due to variations between WPs will not cause local values of t_{bp} to significantly deviate from average conditions.

Repository Temperatures as a Function of Thermal Properties

The next six sub-sections address the sensitivity of thermo-hydrological performance to thermo-hydrological properties and boundary conditions. We begin with a sub-section that examines the sensitivity of thermo-hydrological performance to thermal properties. Past hydrothermal calculations[5] utilized the K_{th} values from the Reference Information Base (RIB) Version 3. In this study we apply the RIB Version 4 values of K_{th}. Because Version 4 values of K_{th} are generally lower than those found in Version 3, all of the Version 4 cases have longer boiling periods. For example, for 30-yr-old SNF with an APD of 57 kW/acre, t_{bp} increases from 1800 to 2075 yr (Fig. 9a). For 30-yr-old SNF and an APD of 114 kW/acre, t_{bp} increases from 5000 to 6503 yr and for 60-yr-old SNF and an APD of 114 kW/acre, t_{bp} increases from 10,000 to 12,629 yr. Note that these comparisons were made with the UZ model (which assumes fixed-depth, constant-temperature water table).

While t_{bp} increases, T_{peak} for the Version 4 cases does not increase. Contrary to the general trend that K_{th} is less in Version 4 than in Version 3, the dry value of K_{th} for the TSw2 (the repository horizon) is considerably greater in Version 4 than in Version 3. Incidentally, the wet value of K_{th} is considerably less in Version 4 than in Version 3. Because the dry value of K_{th} is applicable to the dry-out zone, the Version 4 K_{th} distribution results in greater heat dissipation in the dry-out zone (relative to Version 3), thereby reducing T_{peak}. In the region outside of the boiling zone (including the condensation zone), the applicable K_{th} is much closer to the wet value. Therefore, the lower K_{th} distribution in Version 4 tends to reduce the far-field heat loss, thereby extending t_{bp}.

Repository thermal calculations using heat conduction models have assumed K_{th} for TSw2 can be applied to the entire UZ.[1,2] However, K_{th} (both wet and dry values) for TSw2 are twice as large as the wet K_{th} for the nonwelded PTn and CHnv units and the welded CHnz and nearly four times larger than the dry K_{th} for the CHnz. Therefore, applying the K_{th} of the TSw2 to the entire UZ tends to substantially under-represent the insulating effect of the lower K_{th} values of the far-field units. We repeated our calculations with K_{th} of the TSw2 applied to the entire UZ and found that t_{bp} is reduced by 50% relative to the Version 4 K_{th} distribution. For 30-yr-old SNF and an APD of 114 kW/acre, t_{bp} is reduced from 6503 to 3364 yr (Fig. 9b). For long-term boiling performance, the depth of the repository appears to be optimally located because the highest K_{th} is in the near-field (which lowers T_{peak}), and the lowest K_{th} is in the far-field (which extends t_{bp}).

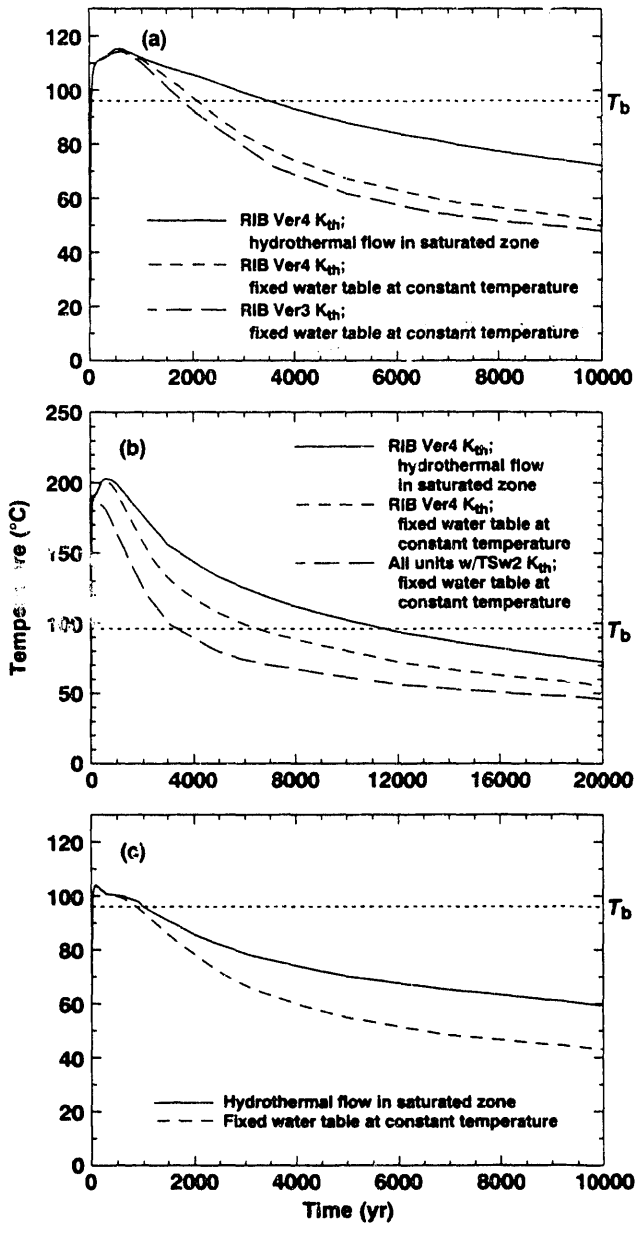

Figure 9. Temperature history at repository center for a net recharge flux of 0 mm/yr. (a) APD = 57 kW/acre and 30-yr-old SNF. (b) APD = 114 kW/acre and 30-yr-old SNF. (c) APD = 57 kW/acre and 10-yr-old SNF (reference SCP-CDR thermal load).

Impact of Saturated Zone Flow on Repository Temperatures

In this sub-section we investigate the impact of hydrothermal flow in the SZ on repository temperatures by comparing results from the UZ model (which assumes a fixed-depth, constant-temperature water table) with those obtained with the UZ-SZ model (which includes hydrothermal flow in the SZ). For all of the cases considered (20 to 114 kW/acre; 30- and 60-yr-old SNF), the treatment of the water table and the SZ has very little impact on repository temperatures during the first 1000 yr (Fig. 9a–c). Because temperatures peak within 1000 yr, T_{peak}, is not affected by the treatment of the water table and SZ. For 30-yr-old SNF and an APD of 57 kW/acre,

T_{peak} is 114.9 and 115.3°C for the UZ and UZ-SZ models, respectively (Fig. 9a). For 30-yr-old SNF and an APD of 114 kW/acre, T_{peak} is 201.6 and 202.9°C for the UZ and UZ-SZ models, respectively (Fig. 9b).

For $t > 1000$ yr (after repository temperatures have peaked), the SZ begins to significantly heat up (Fig. 5a and b), thereby reducing the rate at which heat can flow from the UZ to the SZ. Consequently, the duration of boiling, t_{bp}, substantially increases, particularly for higher Areal Mass Loadings, AMLs, ($t_{bp} \gg 1000$ yr). For lower AMLs ($t_{bp} < 1000$ yr), the increase in t_{bp} is less substantial. For the reference SCP-CDR thermal load (APD=57 kW/acre; 10-yr-old SNF), t_{bp} increases from 553 to 666 yr (Fig. 9c). For 30-yr-old SNF and an APD of 57 kW/acre, t_{bp} increases from 2075 to 3506 yr (Fig. 9a). For 30-yr-old SNF and an APD of 114 kW/acre, t_{bp} increases from 6503 to 11,446 yr (Fig. 9b). For 60-yr-old SNF and an APD of 114 kW/acre, t_{bp} increases from 12,629 to 18,121 yr.

Low AMLs (with $T_{peak} < T_b$) are also affected by the treatment of the water table and SZ. For 30-yr-old SNF and an APD of 20 kW/acre, hydrothermal flow in the SZ extends the duration of time the repository is above 50°C from 2200 to 3600 yr and extends the duration of time the repository is above 40°C from 5060 to 14,150 yr.

Impact of Unsaturated Zone Flow on Repository Temperatures

The primary UZ variables of interest are the bulk permeability, k_b, and the net recharge flux. Because the matrix permeability is so small in most of the hydrostratigraphic units in the UZ, differences in k_b reflect differences in fracture permeability. For 30-yr-old SNF and APDs of 57 and 114 kW/acre, the sensitivity of repository temperatures to k_b is considered for k_b ranging from 1.9×10^{-18}m^2 (no fractures) to 2.8×10^{-13}m^2 (three 100-μm fractures per meter). When no fractures are present, there is no significant boiling because the small matrix permeability results in very large gas-phase pressures, causing a rise in the boiling temperature, ΔT_b. In the analysis of the G-Tunnel heater test[14] the gas-phase pressure, p_g, gradients in large matrix blocks (fracture spacing of 3 m) resulted in p_g being tens of atmospheres above ambient, driving large ΔT_bs, thereby substantially suppressing boiling. When no fractures are present, the very small matrix permeability results in negligible gas-phase flow. The absence of convective and boiling effects results in heat-conduction-dominated heat flow and higher T_{peak} than the case with significant convective flow in fractures and boiling effects (Fig. 10a and b).

In our previous hydrothermal modeling study[5] it was found that for $k_b > 10^{-14}$m^2, the dry-out rate is effectively not throttled by flow resistance in the fractures. For $k_b > 10^{-11}$m^2, it was also found that heat convection, resulting from large-scale, buoyancy-driven, gas-phase flow, begins to influence heat flow. In a modeling study of *in situ* heater tests we found that it is necessary for large-scale, buoyancy-driven, gas-phase, pressure gradients to dominate the local boiling pressure gradients in order for heat convection to have a noticeable effect on overall heat flow.[21] When local boiling pressure gradients (that drive steam away from the boiling zone) are more dominant than large-scale buoyancy-driven gas-phase pressure gradients, the flow of steam is vertically symmetrical about the heated horizon. Because the boiling rate is not throttled for $k_b > 10^{-14}$m^2, increasing k_b above this threshold does not increase the rate at which steam is being generated, but it does increase the tendency for large-scale (i.e., far-field) buoyancy-driven convection cells to develop.

For the heater test calculations, $k_b = 8.3 \times 10^{-11}$m^2 was found to be sufficiently large to allow far-field gas-phase convection to drive 100% of the steam in the boiling zone to the upper condensation zone.[21] Although far-field convection completely dominated the direction of steam flow, heat flow was still dominated by heat conduction,

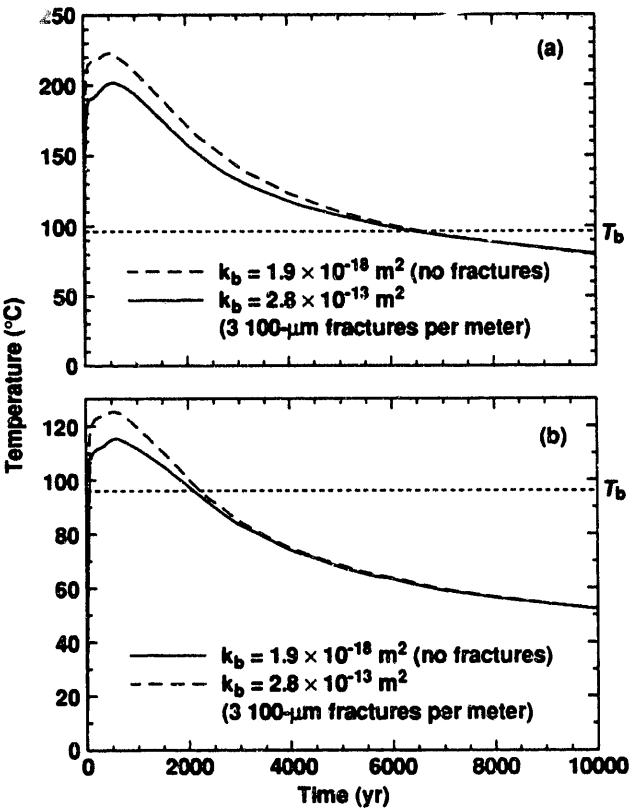

Figure 10. Temperature history at repository center for 30-yr-old SNF, a net recharge flux of 0 mm/yr, and a fixed-depth, constant-temperature water table. (a) APD = 114 kW/acre. (b) APD = 57 kW/acre.

and the duration of the boiling period for the heater test decreased by only 11% relative to the reference case with $k_b = 2.8 \times 10^{-13}$m^2 (the same as the reference case in this study). The effect of heat convection was to enhance heat flow away from the dry-out zone (relative to the case where heat-conduction completely dominated heat flow). Consequently, T_{peak} was reduced from 214.1 to 194.2°C and t_{bp} was reduced from 6.5 to 5.8 yr. Incidentally, for the reference case, local boiling pressure gradients dominate the far-field buoyancy-driven pressure gradients long enough for the flow of steam to be vertically symmetrical about the heated horizon. In general, for 10^{-14}m$^2 < k_b < 10^{-11}$m^2, given sufficiently high AMLs, significant dry-out occurs (unaffected by flow resistance in the fractures or large-scale, buoyancy-driven, gas-phase flow), and thermal performance is relatively insensitive to k_b.

As has been covered in our previous study, contrary to the assumption that the k_b distribution is isotropic and homogeneous, actual fracture distributions show significant variability.[5] In one study, water dripping from fractures was collected along the ceiling of a tunnel complex at Stripa, Sweden.[22] It was found that 50% of the mass flux occurred from 3% of the flow area and that very little flow occurs over 70% of the flow area. It is not certain to what extent this variability in mass flux was due to stresses induced during the mining of the drifts. Generally, a large k_b measurement is the result of flow channeling along a few highly transmissive fracture pathways. Although we assign a homogeneous, isotropic value of k_b in using the ECM, the local value of k_b is probably orders of magnitude smaller than the bulk-averaged value for much of the fractured rock mass.

For 30-yr-old SNF and an APD of 57 kW/acre, t_{bp} is 2075 and 2194 yr for the reference case (three 100-μm fractures per meter) and the case with no fractures, respectively (Fig. 10a). For 30-yr-old SNF and an APD of 114 kW/acre, t_{bp} is 6503 and 6612 yr for the reference case and the case with no fractures, respectively (Fig. 10b). Note that these comparisons were made with the UZ model (which assumes a fixed-depth, constant-temperature water table). Because the rise in ΔT_b suppresses boiling, the cases with no fractures have higher T_{peak}. For 30-yr-old SNF and an APD of 57 kW/acre, T_{peak} is 114.9 and 122.7°C for the reference case (three 100-μm fractures per meter) and the case with no fractures, respectively (Fig. 10a).

For 30-yr-old SNF and an APD of 114 kW/acre, T_{peak} is 201.6 and 222.7°C for the reference case and the case with no fractures, respectively (Fig. 10b). For the case with no fractures, the maximum gas-phase pressure (p_g=22.4 atm) at the repository center occurs at the same time that the temperature peaks (t_{peak}=527 yr). We find in the steam tables[23] that the saturation temperature (equivalent to the boiling temperature) corresponding to p_g=22.4 atm is 218.2°C. Because of the vapor pressure lowering effect due to capillarity, the actual boiling temperature is slightly higher than the saturation temperature in the steam tables. As was observed for the heat pipe effect in the reference case (Fig. 4c), boiling has a pronounced effect on flattening the temperature profile around the nominal boiling temperature, T_b. Because of the large k_b in the reference case, p_g does not increase significantly above the ambient pressure of 0.896 atm at the repository horizon, and the actual boiling temperature coincides with T_b=96°C. In general, until heating can drive the liquid saturation to zero, temperatures will be determined by two-phase thermodynamic equilibrium. In the case of no fractures, high p_gs cause the actual boiling temperature to be much greater than T_b. Because of the very low k_b in the case with no fractures, the thermal load is insufficient to drive water vapor away, thereby lowering the saturation to zero; therefore, temperatures continue to be determined by two-phase thermodynamic equilibrium.

Although T_{peak} is relatively sensitive to whether fractures are present, as long as buoyancy-driven gas-phase flow does not significantly affect the mass flow of steam, t_{bp} is insensitive to whether fracture flow occurs.[21] When buoyancy-driven gas-phase flow dominates the flow of vapor, T_{peak} and t_{bp} are reduced somewhat (but not substantially). For $k_b = 2.8 \times 10^{-13} m^2$, the local boiling pressure gradients dominate far-field buoyancy, resulting in heat-conduction-dominated heat flow for both 57 and 114 kW/acre for 30-yr-old SNF.

The impact of pluvial climatic conditions can be conservatively investigated by assuming a much wetter initial saturation profile. For the low-k_m units, the ECM-calculated saturation profile corresponding to a steady-state net recharge flux of 0.132 mm/yr is at least one standard deviation wetter than the existing RIB data.[8,9] A steady-state net recharge flux of 0.132 mm/yr results in an initial saturation of 95% at the repository horizon as compared to 68% for the reference case of 0 mm/yr (Fig. 1). Given the low k_m of most of the UZ, a transition from the current saturation profile to a profile that would correspond to pluvial climatic conditions may significantly lag behind the change in climatic conditions. Assuming that the transition to the wetter saturation profile has already occurred at the time of emplacement is clearly a conservative means of investigating the impact of a pluvial climate. For 30-yr-old SNF and an APD of 114 kW/acre, we find that in spite of the much wetter initial saturation distribution in the high net recharge flux case, t_{bp} are nearly identical, with t_{bp}=6523 and 6503 yr for the high and nominal net recharge flux cases, respectively (Fig. 11). The high net recharge flux case was associated with lower T_{peak} because of the higher initial volumetric heat capacity of the partially saturated rock, with T_{peak}=175.5 and 201.6°C for the high and nominal net recharge flux cases, respectively (Fig. 11). We also found that the liquid flux associated with condensate drainage back to the boiling zone is much greater than the net recharge flux associated with pluvial climatic conditions. Therefore, it appears that the duration of boiling conditions is insensitive to a wide range of climatic conditions (and associated net recharge fluxes).

In general, it appears that convective effects in either the UZ or SZ are not sufficient to cause the thermal performance of the repository to deviate significantly from being heat-conduction-dominated. Therefore, the duration of boiling, t_{bp}, is primarily sensitive to the thermal properties and thermal loading conditions and much less sensitive to the highly spatially and temporally variable ambient hydrologic properties and conditions. The determination of the thermal properties and thermal loading conditions will be associated with a minor degree of uncertainty and spatial variability. Therefore, with adequate thermal characterization (via *in situ* and laboratory heater testing),[21] the basis for the reliable assessment of thermal performance of the repository can be readily established. Moreover, accurate assessment of repository thermal performance is not dependent on whether boiling results in large-scale dry-out. Therefore, it is not dependent on whether our models are capable of accurately accounting for either large-scale or small-scale movement of water vapor and liquid in the UZ. This is not to say that hydrothermal analysis of vapor and liquid flow is not important to hydrologic performance assessment. The assessment of post-boiling-period hydrologic performance will require assessing the ability of the dry-out zone to mitigate the impact of nonequilibrium fracture flow (under pluvial climatic conditions) on the Engineered Barrier System (EBS) and Natural Barrier System (NBS). Post-boiling-period performance of the dry-out zone will depend on the effectiveness of condensate shedding during the boiling period. The analysis of nonequilibrium fracture flow of condensate and major episodes of recharge will be required to establish the effectiveness of condensate shedding and the robustness of the boiling zone in mitigating the impact of high-flux fracture flow in the UZ.

For high thermal loads (which are able to rely on long-term above-boiling conditions to assure dry WP conditions), the characterization and assessment of EBS and NBS boiling period performance will be insensitive to the highly spatially and temporally heterogeneous distribution of ambient hydrologic properties and conditions. For low or intermediate thermal loads (which do not rely on boiling to assure dry WP conditions), the characterization and assessment of hydrologic performance of the EBS and NBS will be extremely sensitive to the highly spatially and temporally heterogeneous distribution of ambient hydrologic properties and conditions. The hydrologic performance of low or intermediate thermal loads will also depend on the spatial variability in the heat generation rate among the WPs that

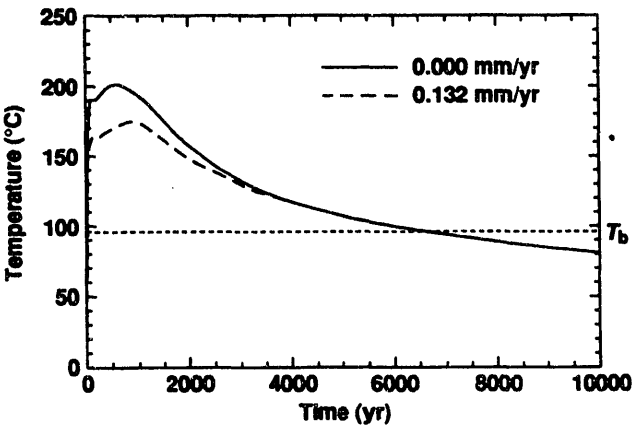

Figure 11. Temperature history at repository center for 30-yr-old SNF, an APD of 114 kW/acre, and a fixed-depth, constant-temperature water table.

drive condensate flow from hotter to cooler WPs. As will be discussed in the following sub-section, repository-heat-driven refluxing even occurs under sub-boiling conditions.

Impact of Refluxing Under Sub-boiling Conditions

The impact of low AMLs (resulting in sub-boiling conditions and negligible dry-out) on repository-heat-driven refluxing was considered for 30- and 60-yr-old SNF and APDs of 20 and 36.2 kW/acre. We found that even for thermal loads for which the average peak temperature never exceeds boiling, repository-heat-driven refluxing will be significant for tens of thousands of years. Under ambient conditions, the geothermal gradient drives ambient refluxing even if the net flow of moisture is zero. Depending on what is assumed for naturally occurring net recharge flux, repository-heat-driven condensate drainage (and ambient refluxing) will probably be the dominant sources of liquid flux in the UZ.

For 30-yr-old SNF and an APD of 36.2 kW/acre (AML=49.2 MTU/acre equivalent to the reference SCP-CDR case of 57 kW/acre and 10-yr-old SNF), the average temperature at the repository center peaks at 89.2°C. Although boiling temperatures never occur, repository-heat-driven refluxing results in as much as a 1 mm/yr of liquid flux at the repository horizon (90 times the ambient refluxing). For 20-yr-old SNF and an APD of 20 kW/acre, repository-heat-driven refluxing is at least five times greater than ambient refluxing. Therefore, boiling conditions are not required to generate significant vapor-phase and liquid-phase flux due to repository heating. Because sub-boiling conditions will also not mitigate the occurrence of deep nonequilibrium fracture flow (from meteoric sources), hydrologic assessments of low AMLs must account for the superposition of naturally occurring episodic fracture flow and repository-heat-driven refluxing for essentially all the time of regulatory concern.

In general, two conditions are required to generate sub-boiling refluxing: liquid water and sufficient thermal gradients. At the repository horizon, there are significant differences between sub-boiling refluxing generated by low AMLs ($T < T_b$ for all time) and sub-boiling refluxing generated by high AMLs subsequent to boiling. Because of the long lag in re-wetting of the dry-out zone subsequent to long-term boiling, the repository horizon will have minimal liquid saturation for tens of thousands of years (Fig. 12d and e). By the time enough liquid water returns to the repository horizon to allow refluxing, the temperature gradients will have declined (Fig. 12f), and the potential for repository-heat-driven refluxing will be substantially reduced. However, because low AMLs are associated with negligible dry-out, sub-boiling refluxing will be facilitated by the availability of liquid water during the time that temperature gradients are steepest (Fig. 4a). Therefore, at the repository horizon, post-boiling-period refluxing for high AMLs (that generate substantial dry-out) will probably be much less than the sub-boiling refluxing associated with low AMLs (which generate negligible dry-out).

Boiling, Dry-out, and Re-wetting Performance

In the previous sub-sections we primarily focused on the thermal performance. In this sub-section we examine the relationship of boiling, vapor and condensate flow to the thermal performance of a high-AML repository (generating long-term boiling and sub-ambient saturation conditions). We also look at the relationship between thermal performance and re-wetting of the dry-out zone.

The boiling, dry-out, and re-wetting performance at the center of a 559-acre repository with an APD of 114 kW/acre and 30-yr-old SNF is examined by plotting the vertical liquid saturation, S_l, and temperature profiles (Fig. 12a–f). The temperature distribution is shown as the heavy solid line and the nominal boiling temperature, T_b, is shown as the light dotted line. Notice that the initial S_l distribution (shown as as the light solid line in Fig. 12a–f), corresponds to a net recharge flux of 0 mm/yr (Fig. 1). The S_l distribution for nonzero times is plotted as the dashed line; the dark shaded areas correspond to S_l greater than initial (condensate zones) and the light shaded areas correspond to S_l less than initial (dry-out zone). Notice that the flattening of the temperature profile coincides with the zone of condensate buildup (Fig. 12a–c). The flattening of the temperature profile above the dry-out zone is primarily attributed to the gravity-driven refluxing, or heat pipe effect, while the flattening of the temperature profile below the repository is attributed to condensate drainage convecting heat away from the boiling zone. Some of the condensate generated below the repository horizon has drained to the water table (Fig. 12a). Above the repository, because nonequilibrium fracture flow is not represented, the ECM does not predict condensate shedding. Consequently, condensation above the dry-out zone is manifested by a saturation build-up that persists for at least 100,000 yr (Fig. 12f). On the basis of the observation of the "hydrothermal umbrella" effect of condensate drainage made during the G-Tunnel test, the ECM probably significantly overpredicts the tendency for hydrothermal perching of condensate above the dry-out zone.

Figure 12b is plotted at the time the repository center reaches its peak temperature (t_{peak}=605 yr). This is also when the vertical extent of the nominal boiling front reaches its maximum, with $T \geq T_b$ from z=88 to 564 m (nearly to the water table). For this report we define the dry-out front as corresponding to where the normalized liquid saturation $\bar{S}_l = 0.9$, where $\bar{S}_l$ is defined as

$$\bar{S}_l = \frac{S_l}{S_{l,init}} \tag{5}$$

where $S_{l,init}$ is the initial liquid saturation. In other words, the dry-out front occurs where s_l is 10% percent drier than ambient. At t=605 yr, the vertical extent of the dry-out zone is 253 m, extending from z=205 to 458 m. Figure 12c is plotted at the time (t=2000 yr) the dry-out zone reaches its maximum vertical extent (372 m), extending from z=133 to 505 m (within 63 m of the water table). Note that most of the zeolitized unit (CHnz) is below ambient saturation. Notice also that the vertical extent of nominal boiling front has collapsed significantly since repository and UZ temperatures had peaked (t_{peak}=605 yr).

The vertical advance and retreat of the nominal boiling and dry-out fronts are shown in Fig. 13a and b. Notice that nominal boiling front advances faster than the dry-out front prior to t_{peak} (Fig. 13a). For $605 < t < 2000$ yr, although the nominal boiling fronts are already retreating, the dry-out zone continues to expand. After 2000 yr, the dry-out fronts begin to retreat, but at a slower rate than the nominal boiling fronts. Because the thermal diffusivity of most of the hydrostratigraphic units in the UZ is much larger than the wetting diffusivity, temperature tends to equilibrate back to ambient conditions much more quickly than does saturation. Notice that it requires nearly 120,000 yr for the repository saturation to re-wet to within 90% of the initial saturation (Fig. 13b). It requires more than 163,000 yr for the repository saturation to re-wet to 100% of the initial saturation.

At t=11,914 yr, although it is 468 yr since the end of the boiling period, the vertical extent of the dry-out zone is still 243 m (Fig. 12d). Long after boiling has ceased, the vertical extent of dry-out is 141 m (t=30,000 yr) and the repository has only re-wetted back to 15.5% saturation (Fig. 12e). As long as boiling persists, naturally occurring fracture-dominated flow is unlikely to penetrate through the dry-out and boiling zones (thereby reaching the WPs and transporting radionuclides). After boiling ceases, the capacity of the UZ to retard naturally occurring fracture-dominated infiltration would continue to

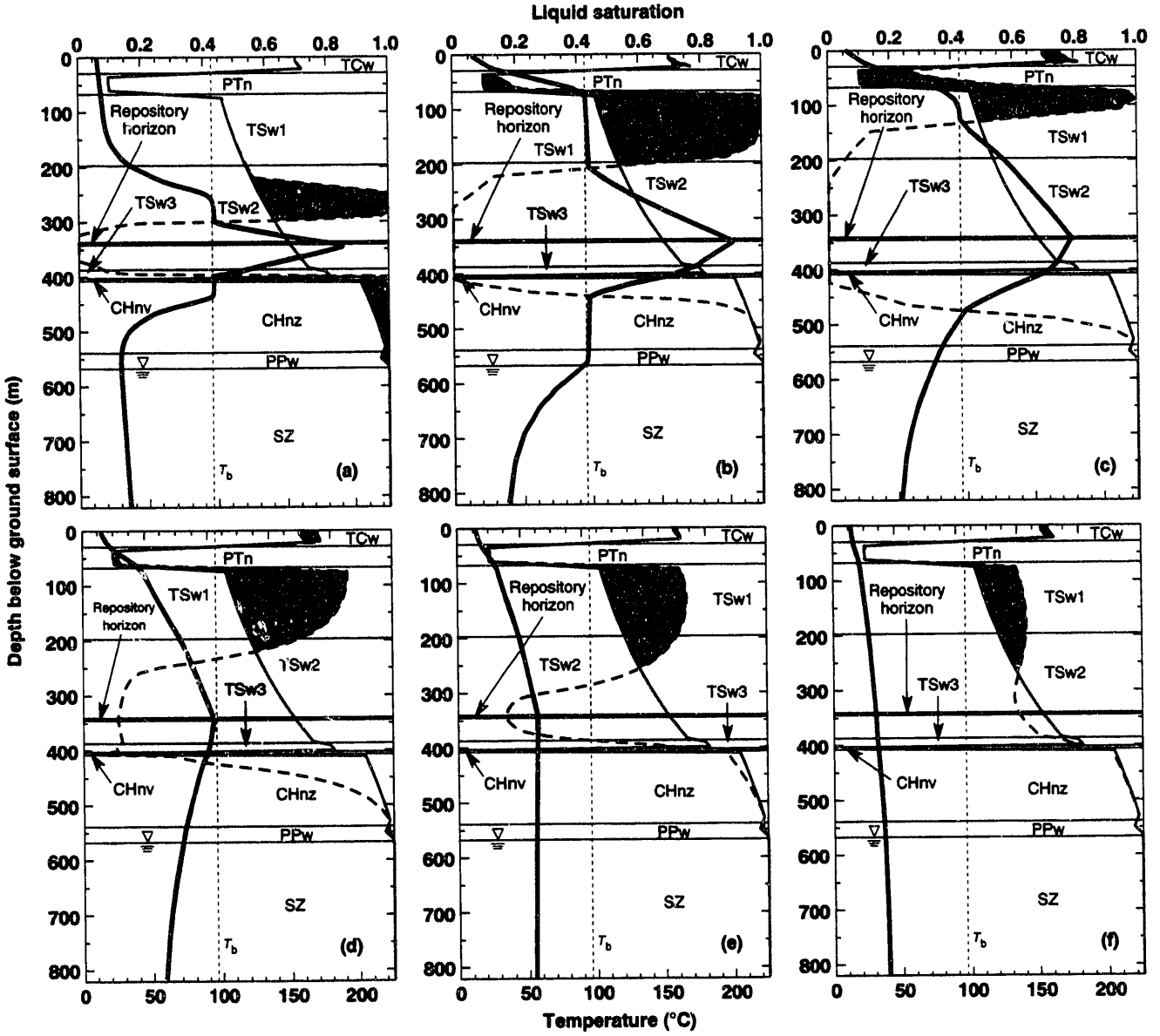

Figure 12. Vertical temperature (heavy solid curve) and liquid saturation (medium dashed curve) profile along repository centerline for 30-yr-old SNF, an APD of 114 kW/acre, and a net recharge flux of 0 mm/yr, including hydrothermal flow in the SZ, at (a) t = 100 yr, (b) t = 605 yr, (c) t = 2000 yr, (d) t = 11,914 yr, (e) t = 30,000 yr, and (f) t = 100,000 yr. Light shaded area indicates depths that are drier than ambient liquid saturation (dry-out zone). Dark shaded areas indicate depths that are wetter than ambient liquid saturation (condensation zones).

be enhanced because of enhanced matrix imbibition within the thick dry-out zone. Moreover, the capacity to retard fracture-to-matrix-to-fracture flow along discontinuous fracture pathways would also be enhanced. This latter effect may be particularly important in the high-k_m units. Under ambient conditions, saturations in the high-k_m units may be quite high. Episodic fracture-dominated flow within such a unit would not require much wetting of the matrix to develop a fracture-to-matrix-to-fracture "bridge." Drying out such a unit would substantially increase the wetting requirements of the matrix before such a "matrix bridge" could be established between two fractures.

For a zero net recharge flux, re-wetting of the dry-out zone had been observed to occur more from below the repository than from above.[5] This observation may not necessarily apply in the case of a very large net recharge flux, which may be associated with pluvial climatic conditions. Much of the re-wetting is driven by capillary imbibition from below the repository, with the saturated zone (SZ) being the primary source of water (Fig. 12d–f). Had the effect of condensate shedding been represented in these calculations, saturations above and below the dry-out zone would be less than that calculated in this study. As long as repository saturations remain below the initial profile (corresponding to gravity-capillary equilibrium), matrix-dominated flow below the repository will continue to be upward, which would tend to transport any radionuclides present in the matrix back toward the repository.

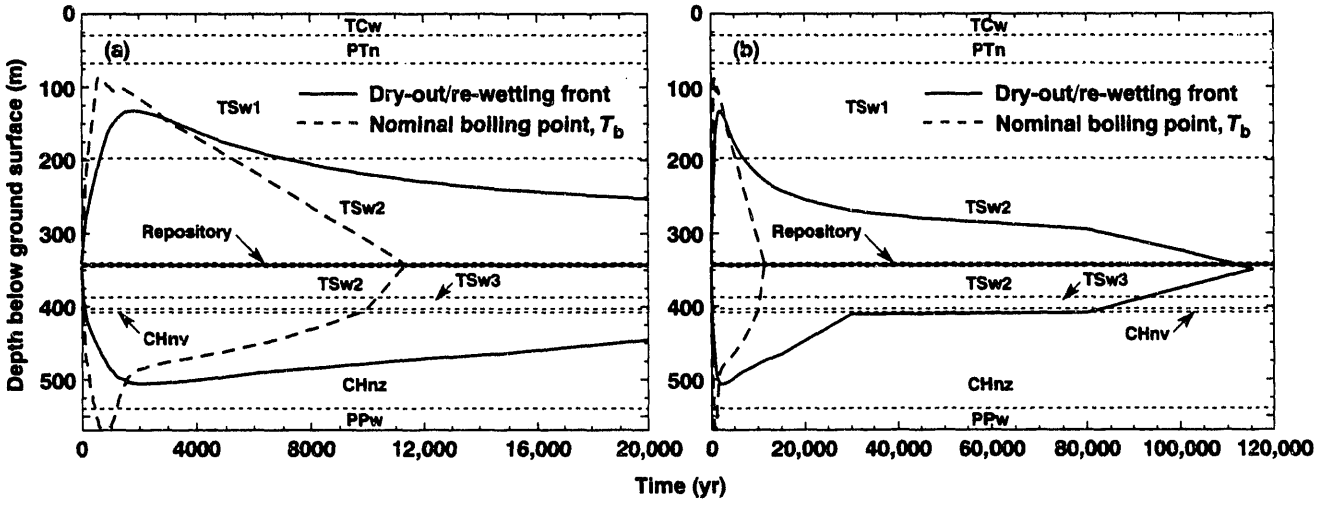

Figure 13. Vertical location of the nominal boiling point front, T_b, and the dry-out/re-wetting front along the repository centerline for 30-yr-old SNF, an APD of 114 kW/acre, and a net recharge flux of 0 mm/yr, including hydrothermal flow in the SZ, during (a) the first 20,000 yr and (b) the first 120,000 yr.

Hydrothermal Flow in the Saturated Zone

In previous sub-sections we investigated the impact of hydrothermal flow in the SZ on thermo-hydrological performance in the UZ. The primary focus in this sub-section is to examine the effects of hydrothermal flow in the SZ on the thermo-hydrologic performance of the SZ itself. We examine the sensitivity of SZ thermo-hydrological performance to thermal loading design parameters as well as to thermo-hydrological properties. We also address the question of whether repository-heat-driven hydrothermal flow in the SZ will dominate the hydrological performance of the SZ. We also begin to investigate the magnitude of heat convective effects on heat flow between the UZ and SZ.

We compare the magnitude of repository-heat-driven buoyancy flow in the SZ for three cases of 30-yr-old SNF having the same total mass of SNF: (1) 20 kW/acre over a repository area of 3162 acres, (2) 57 kW/acre over 1118 acres, and (3) 114 kW/acre over 559 acres. We have observed that temperatures in the SZ build up considerably, even for low thermal loads (Fig. 5a and b). Although heat convection does not dominate heat flow in the SZ, after approximately 1000 years, heat flow in the SZ appears to dominate fluid flow in the SZ. This dominant influence of repository-heat-driven flow was found to occur for all APDs investigated, 20 to 114 kW/acre for 30-yr-old and 60-yr-old SNF. As the SZ temperatures below the repository rise, the accompanying decrease in mass density results in significant upward component of flow from considerable depth, generating buoyancy-driven convection cells.

Repository-heat-driven convection cells in the SZ require tens of thousands of years to fully develop. As the thermal pulse from the repository propagates both vertically and radially into the SZ, the region over which repository-heat-driven convection occurs continues to expand during (at least) the first 20,000 years (Fig. 14a–b and 15a–b). As this region expands, additional parallel convection cells are added to the convective system. After 1000 years, two convection cells have developed (in cross section), extending radially approximately 2-3 km from the repository center (Fig. 14a); after 5000 years, the radial extent of repository-heat-driven convection is about 5 km (Fig. 14b); after 10,000 years, the radial extent of the convection cells is about 8-10 km (Fig. 15a); after 20,000 yr the radial extent of the convection cells exceeds 10 km from the repository center (Fig. 15b). Because the matrix permeability of the SZ is presumably quite small, these large-scale, buoyancy-driven convection cells require large-scale connectivity within the fracture system.

The connectivity and bulk permeability of the fracture system in the SZ will be determined through the analysis of multiple-well, multiple-level, packer tests. However, the use of *in situ* heater tests in the SZ would give us much more direct evidence that the fracture properties in the SZ are sufficient to result in significant buoyancy-driven SZ flow. Because the driving force for buoyancy-driven SZ flow is primarily propagated by heat conduction (rather than by direct hydraulic communication through connected fracture networks), the use of SZ heater tests would provide valuable information about the bulk fracture network properties, which can not be obtained through conventional packer tests. The temperature field acts as a signature for convective effects. Diagnostic thermal probes, which are extremely sensitive to differences between conductive and convective heat flow, would also assist in the interpretation of convective effects.[24] The SZ heater tests would provide a valuable tool in understanding the ambient system as well as how the SZ system responds to heat. Assessing the potential significance of heat-driven convection in the SZ with the use of hydrothermal models that were solely based on packer test data (i.e., without the benefit of SZ heater tests), may be associated with a high degree of uncertainty.

Although the geometric details of the convection cells differed, we found that the overall magnitude of repository-heat-driven buoyancy flow is relatively insensitive to APD. For example, at $t = 5000$ yr, the maximum horizontal fracture velocity, $(v_h)_{max}$, is 1182 m/yr for 20 kW/acre (Fig. 16a), and 1575 m/yr for 114 kW/acre (Fig. 16b). Although the APD varies by a factor of 5.7, the difference in $(v_h)_{max}$ is only 33% between these two cases. Incidentally, for 57 kW/acre, $(v_h)_{max}$ is 1513 m/yr at $t = 5000$ yr (Fig. 14b). The fracture velocity is obtained by multiplying Q_{ECM} by the ratio of the total porosity divided by the fracture porosity. Using the same bulk permeability, k_b, applied in these calculations ($k_b = 2.8 \times 10^{-13}$ m^2), and applying a relatively steep hydraulic gradient of 10^{-3} m/m results in a v_h of only 63 m/yr. Therefore, it appears that repository-heat-driven flow may dominate SZ flow for tens of thousands of years.

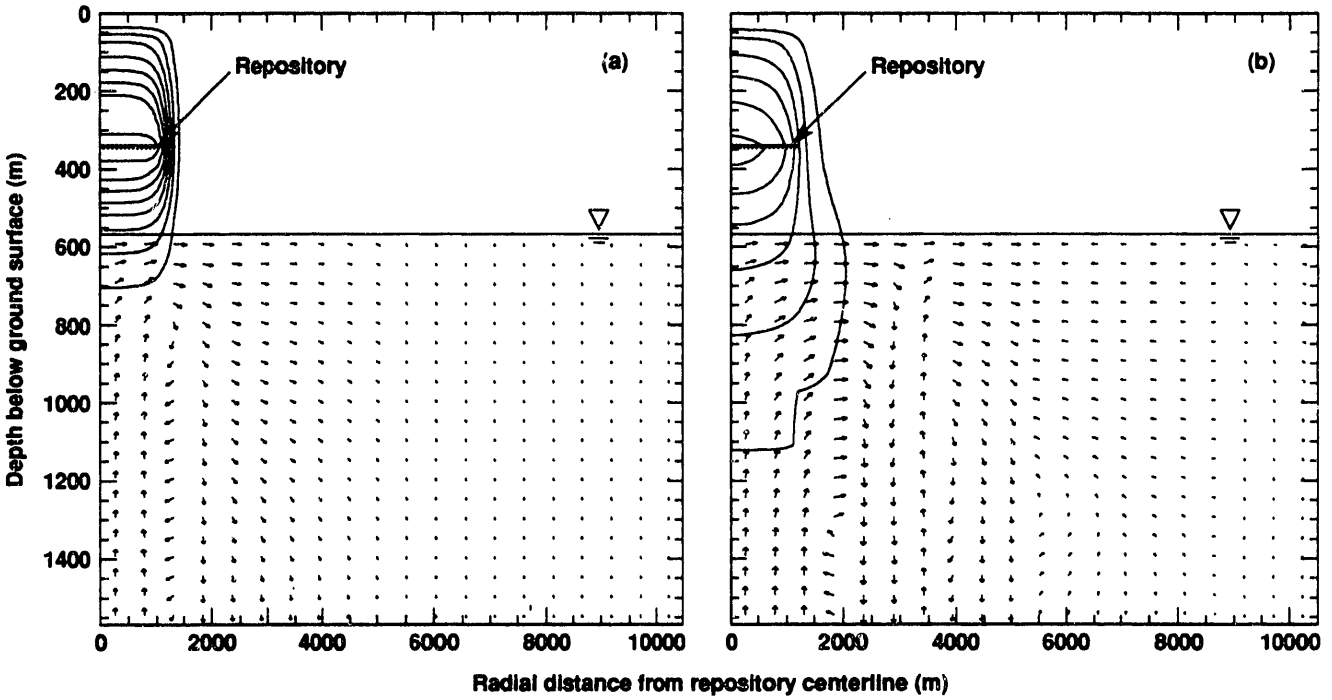

Figure 14. Temperature buildup contours above ambient and fracture velocity field in the SZ for 30-yr-old SNF, an APD of 57 kW/acre, and a net recharge flux of 0 mm/yr, at (a) t = 1000 yr, (b) t = 5000 yr. Temperature contour interval is 5°C. Fracture velocity vectors are scaled logarithmically from 0.03 m/yr to 1600 m/yr.

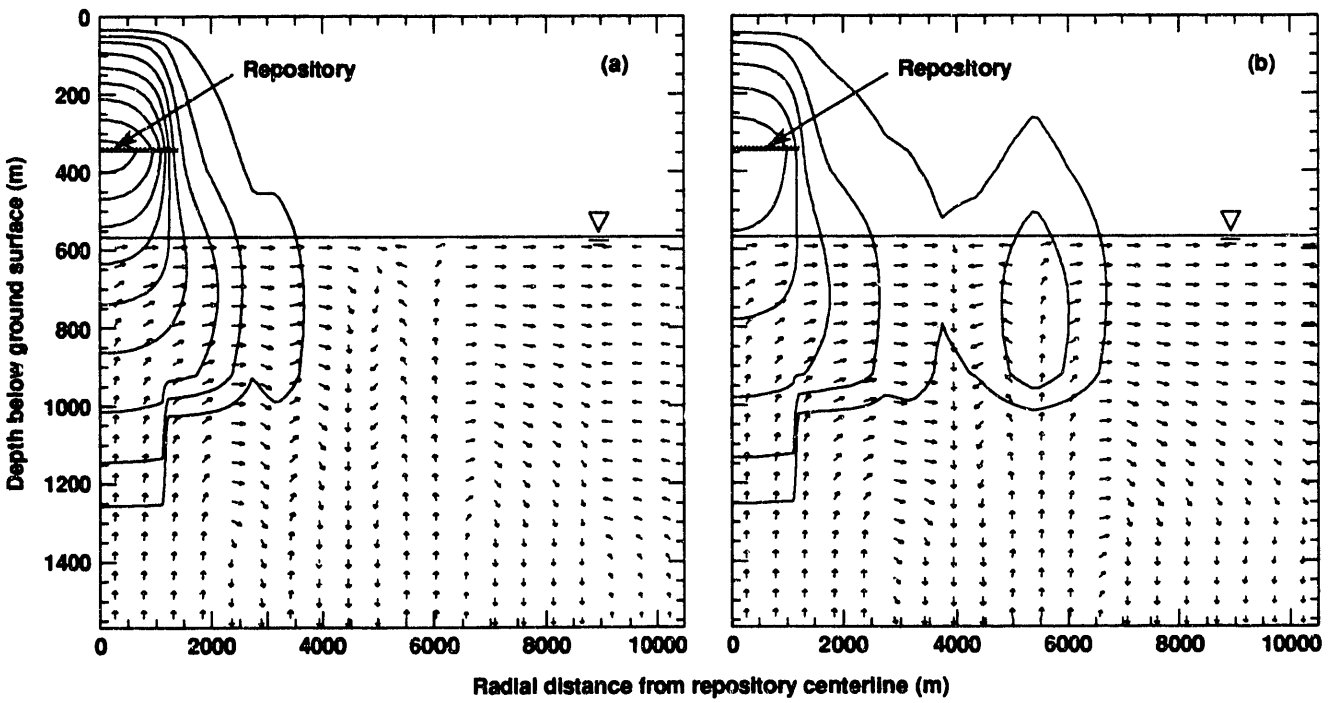

Figure 15. Temperature buildup contours above ambient and fracture velocity field in the SZ for 30-yr-old SNF, an APD of 57 kW/acre, and a net recharge flux of 0 mm/yr, at (a) t = 10,000 yr, (b) t = 20,000 yr. Temperature contour interval is 5°C. Fracture velocity vectors are scaled logarithmically from 0.03 m/yr to 1600 m/yr.

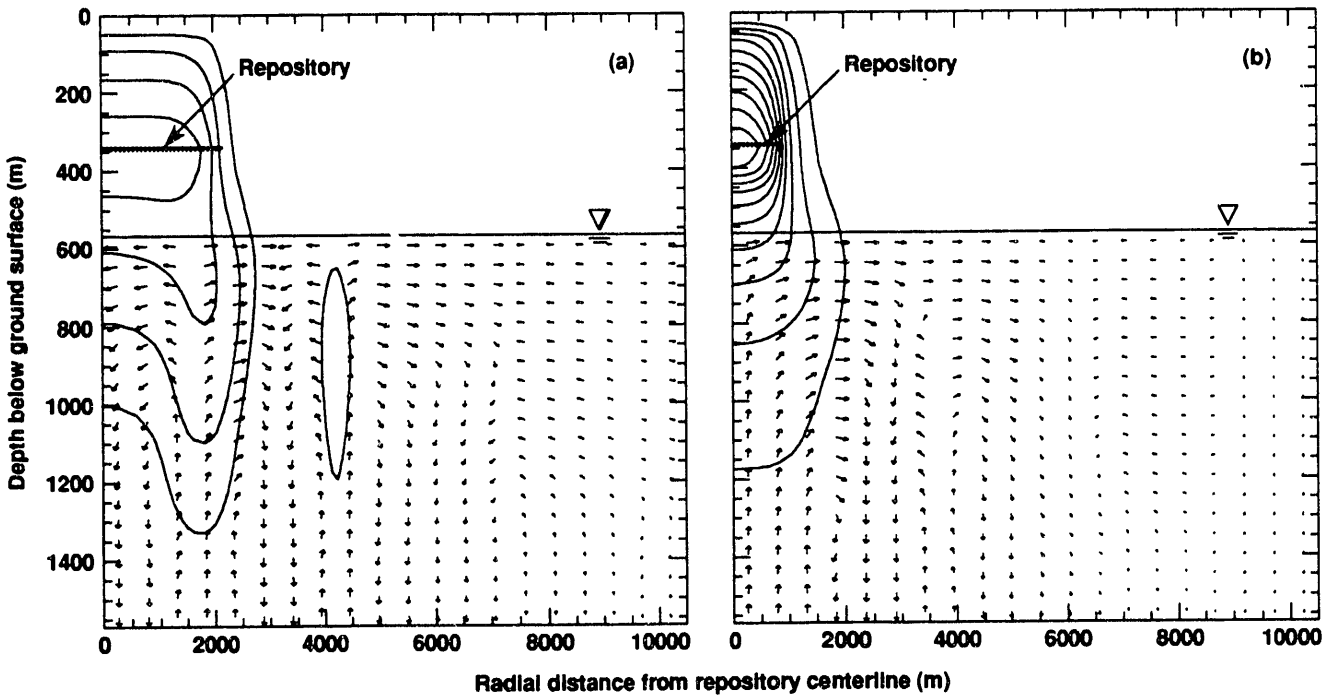

Figure 16. Temperature buildup contours above ambient and fracture velocity field in the SZ for 30-yr-old SNF and a net recharge flux of 0 mm/yr at t = 5000 yr. Fracture velocity vectors are scaled logarithmically from 0.03m/yr to 1600 m/yr. (a) APD = 20 kW/acre and a 3162-acre repository with a temperature contour interval of 5°C. (b) APD = 114 kW/acre and a 559-acre repository with a temperature contour interval of 10°C.

Repository-heat-driven buoyancy flow in the SZ is a result of changes in fluid volume, ΔV, which occur as the region below the repository is heated. Because ΔV increases with ΔT, the magnitude of buoyancy flow generally increases with ΔT. Although ΔV per unit volume of heated SZ is less for lower APD, the larger "footprint" associated with the low APD repository results in a larger overall region where this heat-driven change in volume takes place (compare Fig. 16a and b). Consequently, for a given amount of time-integrated heat, the cumulative effect of repository heating on driving convection cells in the SZ is similar over a wide range of APD. In general, the magnitude of repository-heat-driven buoyancy flow in the SZ is insensitive to the actual design of the repository and is primarily sensitive to the time-integrated heat (i.e., total mass of SNF emplaced in the repository). Consequently, the hydrothermal and potential geochemical consequences of heat in the SZ should not be considered a design issue, but rather the inherent response of the SZ to the emplacement of a given quantity of SNF.

Notice for $t \geq 5000$ yr, the isotherms of the temperature buildup (Figs. 14b, 15a, 15b, 16a, and 16b), show significant deviations relative to what would be expected for heat-conduction-dominated heat flow. These deviations do not arise from the convection of repository heat; instead they are caused by the convection of hotter water from below (hotter because of the geothermal gradient). Because a constant-property boundary is maintained 1 km below the water table and liquid flow is both entering and leaving this boundary, the convection cells are not within a closed loop. Consequently, the boundary effect prevents cooler water that enters the boundary from cooling the warmer water leaving the boundary. Therefore, it is possible that this boundary effect introduces additional heat that would not have occurred had the finite extent of the convection cell been fully represented in our model. On the other hand, the close proximity of a constant-temperature boundary to significant temperature changes has the tendency of artificially lowering temperatures. It is not clear whether the net impact of these two effects causes an overall increase or decrease of heat in the upper 1000 m of the SZ. We analyzed several cases with no fracture flow (effectively causing heat flow to be entirely dominated by heat conduction) and found negligible differences in heat flux crossing the water table. Therefore, the boundary effects which occur 1 km below the water table do not affect UZ temperatures. It should be noted that very little data exist concerning the vertical extent of connected fracture networks in the SZ and that the thermal property data below the PPw unit is lacking in the RIB.[9] We plan to continue our study of repository-heat-driven hydrothermal flow in the SZ, utilizing other available sources of thermal property data.[25]

We also examined the sensitivity of buoyancy-driven SZ flow to bulk permeability, k_b. We found that the threshold k_b for significant buoyancy-driven flow effects occurs somewhere in the range $10^{-16} < k_b < 10^{-13} m^2$. Recall that we had found that the threshold k_b for significant dry-out effects occurs in roughly the same range ($k_b \approx 10^{-14} m^2$). Although there are different phases (liquid-phase vs gas-phase) involved in these convective processes, it is interesting to note that approximately the same threshold k_b applies. It is possible that for hydrostratigraphic units that occur both below and above the water table at Yucca Mountain, heater testing in the SZ could be used to determine whether fracture densities and connectivities are sufficient to promote significant dry-out (due to boiling) in the UZ. Conversely, heater testing in the UZ would indicate whether the fracture properties are conducive to SZ buoyancy flow.

We also considered the sensitivity of our model results to the radial boundary (that assumes the initial pressure, temperature, and saturation distribution remains constant) located at a radial distance, r, of 15 km from the repository center. While this boundary has no

impact on hydrothermal flow in the UZ, a small amount of liquid flows into and out of the outer radial boundary in the SZ for $t \leq 50{,}000$ yr. However, this effect does not affect buoyancy-driven flow for $r < 13$ km. In future work we intend to increase the radial distance to the outer constant-property boundary and increase the depth to the lower constant-property boundary. In general, our analysis indicates that the spatial domain that must be accounted for in the model extends at least 1 km below the water table and at least 15 km radially away from the center of the repository, indicating the extensive spatial extent of repository-heat-driven hydrothermal flow effects.

Major Hydrothermal Flow Regimes and Hydrologic Performance

The validation of performance assessment (PA) models will be expedited by the development of a methodology for demonstrating that critically important features and processes are adequately represented in the detailed hydrological process models that are the basis for the PA models. The critically important hydrological processes, and the necessary level of detail required to represent them, change with time after waste emplacement because of the impact of repository heat. The impact of repository-heat-driven flow on hydrological performance can be described as a series of hydrothermal flow regimes (HFRs). Three major HFRs have been identified: HFR I occurs when boiling (and possibly condensate flow) dominates hydrological performance, HFR II occurs during the sub-boiling period when the fluid distribution and intrinsic hydrological flow and transport properties are still significantly altered by the repository heat, and HFR III occurs in the absence of repository-heat-driven effects on either the fluid distribution or the intrinsic flow and transport properties. Note that the sub-boiling period pertains to either pre-boiling or post-boiling conditions or for regions that never attain boiling conditions.

Each of the first two major hydrothermal flow regimes can be broken into two sub-regimes. HFR Ia occurs when boiling and condensate flow dominate (or significantly influence) hydrological performance. HFR Ib occurs when boiling conditions have coalesced and extend sufficiently far from the WPs so that boiling conditions dominate the hydrological performance of the WP environment. For HFR Ib, liquid-phase fracture flow in the vicinity of the WP is extremely unlikely.

During HFR II, fluid flow is dominated by several possible effects, including (1) residual post-boiling effects of rock dry-out and condensate buildup, (2) repository-heat-driven refluxing under sub-boiling conditions, and (3) property alteration arising from changes in temperature or fluid saturations. These residual repository-heat-driven effects can be divided into two categories: HFR IIa involves the impact of flux change and fluid redistribution (the residual dry-out and condensate zones) and intrinsic property alteration; and HFR IIb involves the repository-heat-driven alteration of the intrinsic properties of the hydrologic-geochemical system (e.g., alteration of matrix permeability, k_m, due to dehydration). HFR IIa persists as long as fluid saturations (and fluxes) are in the process of being re-equilibrated back to a distribution that is dominated by ambient boundary conditions. HFR IIb persists as long as some of the intrinsic hydrologic-geochemical properties (e.g., k_m) remain altered (relative to their pre-emplacement values). The final hydrothermal flow regime, HFR III, pertains to when the fluid saturation and flux distribution are dominated by ambient conditions, and the intrinsic hydrological-geochemical properties have been restored to pre-emplacement values. If the climatic conditions have not changed, HFR III is the same as pre-emplacement ambient flow. It is likely that conditions for HFR III will never be attained within the region that impacts the performance of the EBS and NBS except close to the ground surface.

For thermal loading conditions that generate marginal boiling performance, conditions for HFR Ib will never be attained. Instead there will be a transition from HFR Ia to HFR IIa. For thermal loading conditions that do not generate boiling conditions anywhere within the repository, HFR I cannot occur and hydrothermal performance will commence with HFR IIa.

The hydrothermal flow regimes can be applied anywhere within the EBS and NBS, including in the SZ. They are particularly useful for assessing performance at the WP environment. The HFRs are plotted for WPs at the center of the repository as a function of AML (MTU/acre) and time (Fig. 17), based on the average temperatures predicted by the UZ-SZ model for a wide range of AML scenarios. Therefore, a given thermal loading scenario is represented by a unique value of AML (Fig. 17). Because thermal homogenization takes place prior to the end of the boiling period for high AMLs, the transition from HFR Ib to HFR IIa can be accurately determined on the basis of average repository temperatures. Because thermal homogenization does not take place prior to the end of the boiling period for low to intermediate AMLs, the transition from HFR Ia to IIa cannot be accurately determined on the basis of average repository temperature performance. In order to establish the HFR Ia-to-IIa transition, detailed calculations accounting for the spatial variability of WP heat output are required. Future work involving detailed thermal calculations will address the impact of the spatial variability of WP heat output in order to determine the HFR Ia-to-IIa transition. The spatial heterogeneity in HFRs can then be plotted as a function of position in the repository at various times, or a family of AML-vs-time plots could be generated, adequately covering the anticipated range of thermal loading variability within the repository.

Because the HFR Ia-to-Ib transition occurs prior to the time of thermal homogenization, this transition cannot be determined on the basis of average repository temperature performance. Consequently, we show this transition as a dotted line (Fig. 17), indicating that refinements to its location await future detailed thermal modeling. This transition corresponds to the coalescence of boiling zones between neighboring WPs. The details of WP heat generation aside, the time to boiling coalescence decreases linearly with the overall heating rate (which is proportional to AML). Therefore, for a given WP heat load distribution, we know that the HFR Ia-to-Ib transition has a slope of -1.

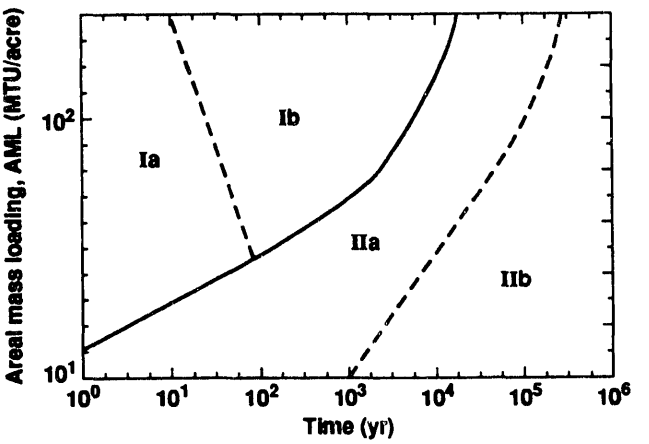

Figure 17. Hydrothermal flow regimes Ia (boiling/condensation-dominated), Ib (above-boiling-dominated), IIa (sub-boiling, thermally-altered flow and thermally-altered intrinsic properties), and IIb (ambient flow and thermally-altered intrinsic properties).

For high AMLs (resulting in a significant rock dry-out zone), the transition from HFR IIa to HFR IIb can be clearly established because it is based on the duration of sub-ambient saturation conditions. We found in this study as in previous work[5] that the time required to re-wet the repository back to ambient saturation conditions is anywhere from 10 to 20 times longer than the duration of the boiling period, t_b. The HFR IIa-to-IIb transition is very sensitive to changes in the hydrologic properties of the fractures and matrix. For example, dehydration of the matrix may cause significant changes in k_m, affecting the re-wetting diffusivity of the dry-out zone. Because there is very little data related to the impact of repository heat on the intrinsic hydrological properties of the UZ, we show the HFR IIa-to-IIb transition as a dotted line. For low to intermediate AMLs (which do not result in significant dry-out effects), the duration of HFR IIa is based on the duration of significant repository-heat-driven refluxing under sub-boiling conditions. Because we have not yet evaluated the threshold for significant refluxing effects, we have tentatively located the HFR IIa-to-IIb transition for low AMLs (Fig. 17).

CONCLUSIONS

This study examined the impact of repository thermal conditions on long-term hydrological performance of the unsaturated zone (UZ) and the upper 1000 m of the saturated zone (SZ) at Yucca Mountain. Hydrothermal flow calculations were conducted with the use of the V-TOUGH code and the Equivalent Continuum Model (ECM) for APDs ranging from 20 to 114 kW/acre and 30- and 60-yr-old SNF with a burnup of 33,000 MWd/MTU. We also considered 21-yr-old SNF (with a burnup of 43,573 MWd/MTU) and 26-yr-old SNF (with a burnup of 39,585 MWd/MTU). Our repository-scale model utilized axisymmetry about the center of the repository, and averaged the thermal load over a 4.6-m-thick disk with a diameter corresponding to the repository area being modeled. Our analysis indicates that the spatial domain, which must be accounted for in the model, extends at least 1 km below the water table and at least 15 km radially away from the center of the repository. Our models include boiling and condensation effects and the convection of latent and sensible heat. In general, these models predict a drying out of the near-field rock by boiling of the vadose water in the rock matrix and the flow of water vapor through fractures to cooler regions, where it condenses. Because of the very low matrix permeability of the host rock, condensate will drain considerable distances along fractures before being totally imbibed by the matrix. The combination of vapor flow away from the heat source and gravity-driven condensate flow down fractures tends to promote shedding of condensate off the top and down the sides of the boiling zone. Below the repository horizon, condensate drains immediately away from the boiling zone, thereby enhancing the dry-out rate. Because the ECM substantially underpredicts the beneficial manner in which condensate shedding enhances rock dry-out, it is conservative with respect to the spatial extent and duration of boiling conditions.

Given that liquid flow along preferential fracture flow paths provides the most likely means of bringing liquid water to WPs and transporting radionuclides to the water table, three general features, or mechanisms, tend to mitigate the potential release and transport of radionuclides. The first is discontinuity in preferential fracture flow paths. The second is liquid-phase dispersion in fracture networks, which results as flow branches from a preferential fracture pathway into lateral fractures. The third mechanism is fracture-matrix interaction. For thermal loading conditions that result in sub-boiling conditions, the predominant mode of fracture-matrix interaction is capillary-driven fracture-to-matrix flow, called matrix imbibition. For APDs resulting in marginal boiling conditions, the variability in the heat generation rate among the WPs may result in condensate flow from hotter to cooler WPs (and possibly to the water table), increasing the adverse effects of fracture flow.

For higher APDs, the resulting large region of above nominal boiling temperatures makes fracture flow at the repository horizon extremely unlikely. We also find that it is unlikely that convective flow effects will be sufficient to cause heat flow to deviate from being heat-conduction-dominated. Moreover, the duration of the boiling period is found to be insensitive to net recharge flux (even for pluvial climate conditions) and to whether large-scale rock dry-out occurs. Therefore, under boiling conditions, hydrologic performance is governed by the system's thermal loading conditions and thermal properties. These factors can be more readily determined and are much less variable than many of the parameters associated with the ambient hydrogeological system. Moreover, the thermal properties are relatively insensitive to hydrothermally driven geochemical effects. Because the thermal diffusivity is much larger than the re-wetting diffusivity of most of the UZ, temperature tends to equilibrate back to ambient conditions much more quickly than does matrix saturation. Consequently, the matrix saturation within the dry-out zone extending above and below the repository horizon will remain below ambient long after boiling has ceased. Sub-ambient matrix saturations will add to the capacity of the UZ to retard fracture flow during the post-boiling-period.

The characterization and assessment of fracture flow retardation under sub-boiling or ambient conditions in the UZ at Yucca Mountain are extremely formidable. The main problems arise from the very nonlinear dependence of fracture flow on the highly heterogeneous distribution of fracture and matrix properties, the uncertainty in characterizing net recharge flux under either current or future (pluvial) climate conditions, and the impracticality of incorporating the complex details of variable aperture fracture networks in numerical models.

Depending on the number of fuel assemblies per WP and variations in the WP heat output, local boiling conditions can persist for hundreds of years even if average repository temperatures appear to be indicative of sub-boiling conditions. Depending on what is eventually determined for the net recharge flux, the liquid-phase flux associated with sub-boiling refluxing may be large relative to the naturally occurring infiltration. Therefore, even for thermal loading scenarios that entirely avoid boiling conditions, repository-heat-driven hydrothermal flow will significantly impact flow in the UZ. Repository-heat-driven buoyancy flow is also found to dominate ambient flow in the SZ. The magnitude of repository-heat-driven buoyancy flow in the SZ is far more dependent on the total mass of emplaced spent nuclear fuel (SNF) than on the details of SNF emplacement, such as the APD or SNF age. Consequently, the hydrothermal and potential geochemical consequences of heat in the SZ should not be considered a design issue, but rather the inherent response of the SZ to the emplacement of a given quantity of SNF. Even for low thermal loading scenarios, the effects of repository-heat-driven condensate drainage, buoyancy flow in the SZ, and elevated temperatures are likely to result in geochemical changes that may significantly alter the flow and transport properties of the natural barriers in both the UZ and SZ.

We find for high AMLs (resulting in long-term boiling and sub-ambient saturation conditions) that liquid-phase flux associated with vapor flow and condensate drainage during the boiling period as well as re-wetting of the dry-out zone during the post-boiling-period is much greater than the net recharge flux associated with pluvial climatic conditions. Even for low AMLs (resulting in insignificant dry-out due to boiling), repository-heat-driven hydrothermal flow will dominate UZ and SZ flow. Therefore, the most important consideration in determining whether the Yucca Mountain site is suitable for the emplacement of heat-producing, high-level nuclear waste is how heat moves fluid that is already present at Yucca Mountain; the impact of water that has yet to infiltrate at Yucca Mountain is of

secondary importance for high AMLs, and is, at best, of equal importance for low AMLs.

Because of the dominance of repository-heat-driven hydrothermal flow, pre-emplacement groundwater travel time has no physical relevance to hydrological performance. Moreover, conditions that are conducive to deep nonequilibrium fracture flow in the UZ also benefit rapid shedding of condensate away from the boiling zone, thereby promoting effective rock dry-out. Therefore, fast groundwater travel times in the UZ would be indicative of a site that is well suited for an extended-dry repository concept. On the other hand, it is possible (although unlikely) that we might find that fractures in the UZ are either too sparse or too poorly connected to promote either deep fracture flow (from meteoric sources) or large-scale dry-out. The absence of large-scale dry-out is not indicative of unsuitable conditions because the same conditions that prevent large-scale dry-out will also prevent deep fracture flow (from meteoric sources). Therefore, the groundwater travel time in the UZ does not discriminate whether conditions are suitable or unsuitable for an extented-dry repository concept.

The licensing of a sub-boiling or marginal-boiling repository will be critically dependent on characterizing the highly heterogeneous distribution of fracture and matrix properties as well as the highly spatially and temporally variable distribution of net recharge flux. Licensing will also depend on validity of hydrological models which account for (1) these very complex, variable distributions, (2) the strongly nonlinear dependence of fracture flow on these heterogeneous distributions, (3) how the spatial variability in the heat generation rate among the WPs will drive condensate flow from hotter to cooler WPs (and possibly to the water table), and (4) the impact of hydrothermal-geochemical coupling on the flow and transport properties as well as on the chemistry of water contacting WPs. Because sub-boiling or marginal-boiling conditions will not mitigate the occurrence of deep nonequilibrium fracture flow (from meteoric sources), hydrologic assessments of low thermal loading conditions must account for the superposition of naturally occurring episodic fracture flow and repository-heat-driven refluxing for essentially all the time of regulatory concern.

The licensing of an extended-dry repository can be based on three fundamental considerations: (1) the spatial and temporal extent of above-boiling conditions, (2) how closely the dry-out zone corresponds to the zone of above-boiling conditions, and (3) how long it takes the dry-out zone to re-wet back to ambient saturation. The validation of the performance of the extended-dry concept is greatly facilitated by addressing several fundamental hypotheses tests: (1) whether heat conduction dominates heat flow, (2) whether fracture density and connectivity are sufficient to promote rock dry-out due to boiling, and (3) whether re-wetting of the dry-out zone significantly lags behind the end of the boiling period. In addressing these hypotheses, we will also ask whether hydrothermal-geochemical-geomechanical coupling must be dynamically accounted for in performance models or whether these coupling effects can be conservatively accounted for by bounding analyses. The use of these hypotheses tests can greatly focus the critical characterization, modeling, laboratory and *in situ* testing activities required in building robust site suitability and licensing arguments. The validation of these hypotheses will profoundly reduce the impact of hydrogeological uncertainty and variability on the predictability of total system performance.

The most conclusive means of testing these hypotheses involves large-scale *in situ* heater tests at various hydrostratigraphic intervals of the UZ.. *In situ* heater tests will also be extremely useful in determining whether temperature rise, condensate flow, and buoyancy-driven SZ flow can drive geochemical changes that significantly alter properties within the EBS and NBS. Critical performance issues involving hydrothermal-geochemical-geomechanical coupling cannot be entirely resolved either in the laboratory or through modeling. Moreover, critical hydrological performance issues cannot be entirely resolved by ambient property measurements conducted during site characterization. Therefore, *in situ* heater tests at various hydrostratigraphic intervals (above as well as below the repository horizon) will be critical to addressing such issues.

Acknowledgments

The authors acknowledge the helpful suggestions of Jim Blink during the past year and the review of Lee Younker. We also appreciate the assistance of Rick Wooten, who prepared the graphics, and the editorial assistance of Sue Stull. This work was supported by the Near-field Hydrology Task (WBS 1.2.2.2.2) of the Yucca Mountain Site Characterization Project. Work performed under the auspices of the U.S. Department of Energy by Lawrence Livermore National Laboratory under Contract W-7405-Eng-48.

References

1. Ryder, E. E., "Results of Two-Dimensional Near-Field Thermal Calculations in Support of M&O Study on Repository Thermal Loading," (1992).

2. Ruffner, D., G.L. Johnson, E.A. Platt, J.A. Blink, and T. Doering, "Drift Emplaced Waste Package Thermal Response," American Nuclear Society, *Proceedings Fourth High-Level Radioactive Waste Management Conference*, Las Vegas, April (1993).

3. Nitao, J.J., "Numerical Modeling of the Thermal and Hydrological Environment Around a Nuclear Waste Package Using the Equivalent Continuum Approximation: Horizontal Emplacement," *UCID-21444*, Lawrence Livermore National Laboratory, Livermore, CA, (1988).

4. Tsang, Y.W., and K. Pruess, "A Study of Thermally Induced Convection Near a High-Level Nuclear Waste Repository in Partially Saturated Fractured Tuff," *LBL-21311*, Lawrence Berkeley Laboratory, Berkeley, CA (1986).

5. Buscheck, T.A., and J.J. Nitao, "The Impact of Thermal Loading on Repository Performance at Yucca Mountain," American Nuclear Society, *Proceedings Third International High-Level Radioactive Waste Management Conference*, Las Vegas, NV, April 12-16, 1992. Also, *UCRL-JC-109232*, Lawrence Livermore National Laboratory, Livermore, CA, (1992).

6. Montazer, P., and W.E. Wilson, "Conceptual Hydrologic Model of Flow in the Unsaturated Zone, Yucca Mountain, Nevada," Water Resources Investigation Report 84-4345, U.S. Geological Survey (1984).

7. Klavetter, E.A., and R.R. Peters, "Estimation of Hydrologic Properties of an Unsaturated Fracture Rock Mass," *SAND84-2642*, Sandia National Laboratories, Albuquerque, NM (1986).

8. Buscheck, T.A., J.J. Nitao, and D.A. Chesnut, "The Impact of Episodic Nonequilibrium Fracture-Matrix Flow on Geological Repository Performance," *Proceedings American Nuclear Society Topical Meeting on Nuclear Waste Packaging (Focus 91)*, Las Vegas, NV, Sept. 30-Oct. 2, 1991. Also, *UCRL-JC-106759*, Lawrence Livermore National Laboratory, Livermore, CA, 1991.

9. DOE (U.S. Dept. of Energy), "Yucca Mountain Project Reference Information Base," *YMP/CC-0002 (Version 04.002)*, Nevada Operations Office, Las Vegas, NV (1990).

10. Nitao, J.J., "Theory of Matrix and Fracture Flow Regimes in Unsaturated, Fractured Porous Media," American Nuclear Society, *Proceedings Second High-Level Radioactive Waste Management Conference*, Las Vegas, NV, April 28-May 2 1991. Also, *UCRL-JC-104933*, Lawrence Livermore National Laboratory, Livermore, CA (1991).

11. Norris, A.E., "The Use of Chlorine Isotope Measurements to Trace Water Movements at Yucca Mountain," *Proceedings American Nuclear Society Topical Meeting on Nuclear Waste Isolation in the Unsaturated Zone (Focus 89)*, Las Vegas, NV, Sept. 17-21, 1989.

12. Ramirez, A.L., T.A. Buscheck, R. Carlson, W. Daily, K. Lee, W. Lin, N. Mao, T.S. Ueng, H. Wang, and D. Watwood, "Prototype Engineered Barrier System Field Test (PEBSFT) Final Report," *UCRL-ID-106159*, Lawrence Livermore National Laboratory, Livermore, CA (1991).

13. Buscheck, T.A., and J.J. Nitao, "Estimates of the Width of the Wetting Zone Along a Fracture Subjected to an Episodic Infiltration Event in Variably Saturated, Densely Welded Tuff," *UCID-21579*, Lawrence Livermore National Laboratory, Livermore, CA (1988).

14. Buscheck, T.A., and J.J. Nitao, "Modeling Hydrothermal Flow in Variably Saturated, Fractured, Welded Tuff During the Prototype Engineered Barrier System Field Test of the Yucca Mountain Project," *Proceedings of the Fifth NRC Workshop on Flow and Transport through Unsaturated Fractured Rock*, University of Arizona, Tuscon, AZ, Jan 7-10, 1991, Also, *UCRL-ID-106521*, Lawrence Livermore National Laboratory, Livermore, CA (1991).

15. Roseboom, E.H., Jr., "Disposal of High-level Nuclear Waste above the Water Table in Arid Regions," *U.S. Geological Survey Circular 903* (1983), 21 p.

16. Nitao, J.J., "V-TOUGH - An Enhanced Version of the TOUGH Code for the Thermal and Hydrologic Simulation of Large-Scale Problems in Nuclear Waste Isolation," *UCID-21954*, Lawrence Livermore National Laboratory, Livermore, CA (1989).

17. Pruess, K. "TOUGH User's Guide," *NUREG/CR-4645*, Nuclear Regulatory Commission (1987).

18. Buscheck, T.A., and J.J. Nitao, "Estimates of the Impact of Drilling Water on Core Samples Taken from Partially Saturated, Densely Welded Tuff," *UCID-21294*, Lawrence Livermore National Laboratory, Livermore, CA (1987).

19. Peters, R.R., E.A. Klavetter, I.J. Hall, S.C. Blair, P.R. Hellers, and G.W. Gee, "Fracture and Matrix Hydrologic Characteristics of Tuffaceous Materials from Yucca Mountain, Nye County, Nevada," *SAND84-1471*, Sandia National Laboratories, Albuquerque, NM (1984).

20. SNL (Sandia National Laboratories), "Site Characterization Plan - Conceptual Design Report," *SAND84-2641*, Sandia National Laboratories, Albuquerque, NM (1987).

21. Buscheck, T.A., and J.J. Nitao, "Large-Scale In Situ Heater Tests for the Characterization of Hydrothermal Flow at Yucca Mountain," American Nuclear Society, *Proceedings Fourth International High-Level Radioactive Waste Management Conference*, Las Vegas, NV, April 1993. Also, *UCRL-JC-112445*, Lawrence Livermore National Laboratory, Livermore, CA, (1993).

22. Neretnieks, I., H. Abelin, and L. Birgersson, "Some Recent Observations of Channeling in Fractured Rocks - Its Potential Impact on Radionuclide Migration," *Proceedings of GEOVAL Conference*, Stockholm, Sweden (1987).

23. Keenan, J.H., F.G. Keyes, P.G. Hill, and J.G. Moore, *Steam Tables: Thermodynamic Properties of Water Including Vapor, Liquid, and Solid Phases*, John Wiley and Sons, Inc, New York, NY (1969).

24. Danko, G., and T.A. Buscheck, "The Use of Single Hole Thermal Probes for Hydrothermal Characterization at Yucca Mountain," American Nuclear Society, *Proceedings Fourth International High-Level Radioactive Waste Management Conference*, Las Vegas, NV, April (1993).

25. Sass, J.H., A.H. Lachenbruch, W.W. Dudley, Jr., S.S. Priest, and R.J. Munroe, "Temperature, Thermal Conductivity, and Heat Flow Near Yucca Mountain, Nevada: Some Tectonic and Hydrologic Implications," *U.S. Geological Survey Open File Report 87-649*, (1988).

END

DATE
FILMED
4 / 30 / 93